



Urban Areas mapping

Algorithm Theoretical Basis Document (ATBD)

Collection 10.0 - ATBD Version 2

Team authors

Breno Malheiros de Melo	USP/EESC
Edimilson Rodrigues dos Santos Junior	USP/EESC
Eduardo Felix Justiniano	USP/FFLCH
Julia Cansado	USP/FAU
Julio Cesar Pedrassoli	UFBA/POLI
Mayumi Hirye	USP/FAU
Talita Micheleti	USP/FAU

Collaborators

Fabio Mariz Gonçalves	USP/FAU
João Meyer	USP/FAU
Marcelo Montañó	USP/EESC
Marcos Roberto Martines	UFSCAR

São Paulo, 2025

Summary	
Summary	1
1. Overview	2
2. Landsat image mosaics	3
3. Classification based on Random Forest algorithm	4
3.1. Spatial scope	4
3.2. Samples collection	4
3.3. Classification algorithm	8
3.3.1. Samples selection	9
3.3.2. Feature Space	9
3.3.3. Random Forest training and classification	10
3.3.4. Temporal smoothing	11
3.3.5. Urban areas binary classification	12
4. Post-classification procedures	12
4.1. Gap fill	13
4.2. Temporal filter	14
4.3. Spatial filter	16
5. Comparison with previous collections	17
6. Validation Strategies	19
6.1. Accuracy Analysis	19
6.2. Comparison with reference maps	20
7. Urban Module	22
7.1. Urban Vegetation	22
7.1.1. Procedures	23
7.1.1.1. Vacant urban spaces (voids) map	23
7.1.1.2. Preliminary Urban Vegetation Map	24
7.1.1.3. Temporal and spatial filters	25
7.1.1.4. Final data assembly	26
7.1.2. Results	27
7.1.3. Comparison with other datasets	30
7.2. Urbanization periods	32
7.3. Urban Slope	32
7.4. Height above nearest drainage	33
8. References	33
Supplemental material	36

1. Overview

This document presents the methodology developed to map urban areas across the Brazilian territory from 1985 to 2024, as part of Collection 10 of the MapBiomias Project. Building on the general MapBiomias framework, the urban area mapping process applies supervised classification using the Random Forest algorithm (Breiman, 2001) and annual composite Landsat imagery.

The methodological workflow comprises three main steps: (i) mosaic generation, to obtain annual composites from Landsat imagery; (ii) probability classification, which includes sample preparation, training of classification models, prediction of class probabilities, and application of thresholds for binary urban/non-urban classification; and (iii) post-classification procedures, encompassing spatial and temporal filtering to improve classification consistency and minimize errors. Subsequently, classification results are exported to the MapBiomias workspace for integration with other thematic classifications within the broader land cover and land use mapping framework (**Figure 1**). Details about each step are provided further and were conducted using Google Earth Engine platform, javascript and python. The codes are openly available in the MapBiomias GitHub repository.

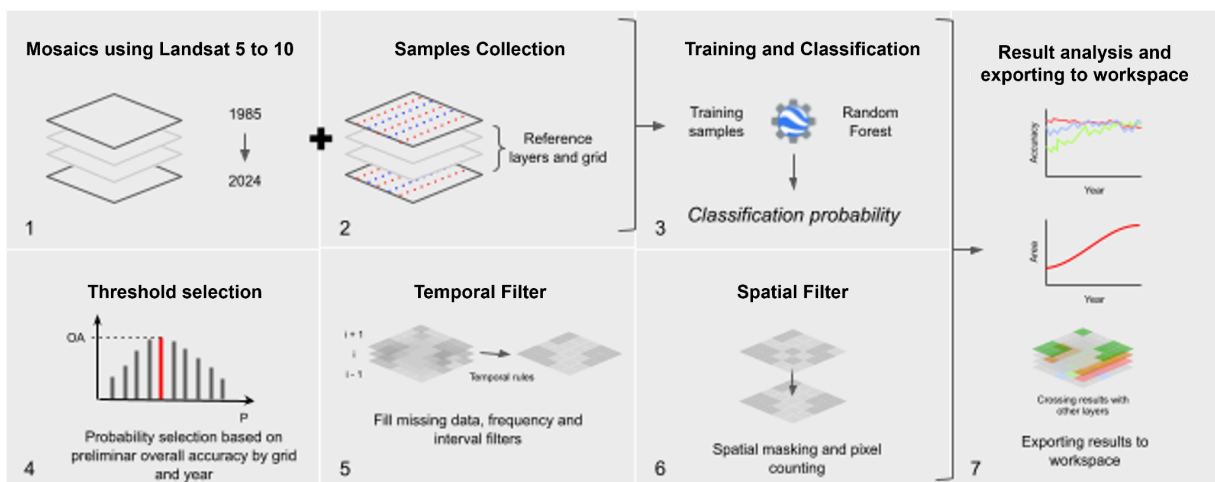


Figure 1. Basic scheme of urban areas classification.

Over successive collections, the urban classification method has been continuously refined through conceptual and methodological improvements. For Collection 10, updates include procedures for training sample selection, and probability thresholding for urban classification. Additional enhancements were made to improve the temporal consistency of the results and reduce classification noise, including the use of a temporal smoothing, probability threshold optimization.

Post-processing steps, including temporal and spatial filtering, were revised in this collection. The main changes compared to previous versions include (i) the reordering of the filter application sequence, with the temporal filter applied prior to the spatial filter; (ii) a simplified and less aggressive temporal filter design to better preserve legitimate temporal dynamics; and (iii) an updated spatial filtering approach, enabling control over the size of spatial artifacts, such as isolated misclassified pixels and small internal gaps while incorporating new auxiliary datasets to enhance spatial consistency.

Since Collection 6, the mapped class has been designated as "Urban/Urbanized Area" (UA), replacing the previous label "Urban Infrastructure". This update aligns the nomenclature with terminology commonly used in urban studies, including by IBGE (2017). UA are areas with predominance of significant density of buildings, roads and infrastructure. It should be noted that when making external quantitative comparisons, it is crucial to ensure that the chosen concepts are aligned.

2. Landsat image mosaics

Landsat imagery was used throughout the time series, incorporating data from Landsat missions 5, 7, 8, and 9 (see supplementary table **ST1**). Both Surface Reflectance products from each mission were used to compute spectral indices, which were then aggregated annually using median values, percentiles, or composite indices (see supplementary **ST2**).

Image processing was conducted using annual image collections. For each year, clouds and shadows were masked, scale factors were applied. Spectral indices were computed as additional bands, based on previous Urban Areas mapping products and existing literature. To reduce pixel values within each year into representative values, appropriate statistical reducers based on selected percentiles were applied. Additionally, differences between percentile values were calculated to capture intra-annual variability. The main processing steps were as follows:

1. Filter Landsat Collection scenes by acquisition date on a yearly basis (from 1985 to 2024) and spatially constrained to the Brazilian territory.
2. Mask cloud and cloud shadow pixels in all scenes using quality attributes derived from the CFMASK 2 algorithm¹, accessed through the QA_PIXEL band.
3. Scale surface reflectance values were scaled to the 0–1 range by applying the provided scale factor (–0.2) and offset (0.0000275) as specified in collections' bands description in each reference page.
4. Compute selected spectral indices and spectral mixture fractions for each scene (see supplementary **ST2**).
5. Apply appropriate reducers to each band and index (see supplementary **ST2**).
6. Calculate differences between reduced indices to capture intra-annual variability (see supplementary **ST2**).
7. Composite all processed bands and indices to produce a single annual mosaic.

The selection of bands and indices for urban area classification was analyzed based on the best-performing classification results (see Section "[Classification algorithm](#)").

¹ CFMask is a multi-pass algorithm that uses decision trees to prospectively label pixels in the scene; it then validates or discards those labels according to scene-wide statistics. It also creates a cloud shadow mask by iteratively estimating cloud heights and projecting them onto the ground. Reference: <https://www.usgs.gov/core-science-systems/nli/landsat/cfmask-algorithm> .

3. Classification based on Random Forest algorithm

Urban areas classification procedures were developed within Google Earth Engine (GEE) based on Landsat imagery and Random Forest algorithm covering the Brazilian territory. The process was divided into several steps, starting with a definition of a spatial scope, satellite imagery, ancillary datasets, and the classification algorithm. This stage was based on selecting the optimal features to provide a temporal consistent urban binary annual classification from 1985 to 2024.

3.1. Spatial scope

This work covers the entire Brazilian territory. However, to avoid unnecessary computation, regions with no signs of urbanization were excluded. Polygons where urban areas are likely to be found were based on existing census tracts (IBGE, 2020). The resulting “search area” was defined using a grid of hexagons that intersect these features, along with topographic sheet codes derived from the World at the Millionth series, scaled to 1:250,000. This regular grid, historically adopted by official agencies for national mapping, were used here as processing units for organizing the computational workflow for urban area mapping (see **Figure 2**).

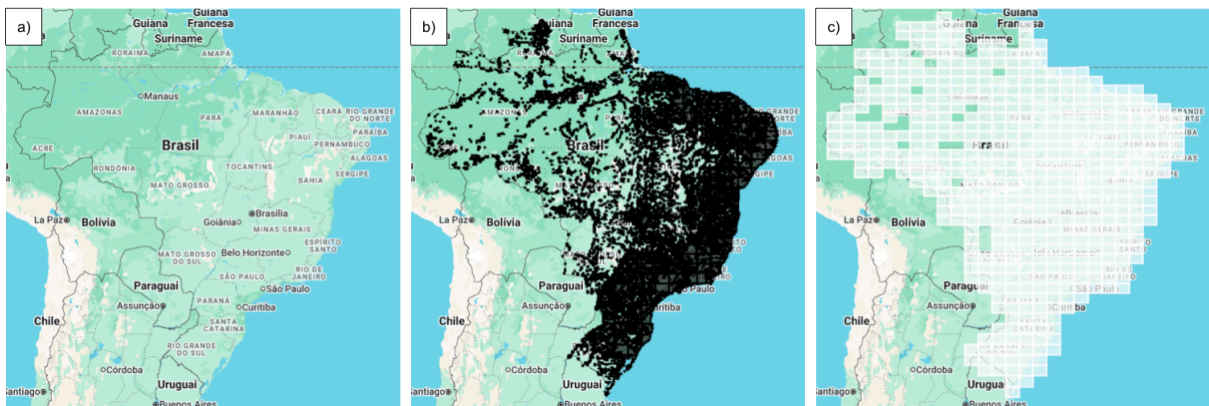


Figure 2. Search area and regular sheets (processing tiles).

a) Brazil. b) Search area - where urban areas can be found. c) Processing units - regular grid defining the tiles for processing the classification.

3.2. Samples collection

Training samples were obtained from the OpenStreetMap database (OSM, 2021), combined with nightlight imagery from NOAA, land cover and land use maps from the Third National Inventory (MCTI, 2015), and built-up area maps from the Global Human Settlement Layer (GHSL), provided by the Joint Research Centre (JRC) (Corbane *et al.*, 2018).

First, a preliminary urban mask was generated based on polylines from OpenStreetMap, representing roads, streets, sidewalks, and unclassified routes contributed by users. Pathways located within urban patches or specific categories (such as residential, service, path, and living street) were selected. To refine this initial mask, pathways outside urban areas were removed using nightlight imagery (NOAA) (**Figure 3**). For selected years, additional filtering was applied using GHSL built-up maps for 1985 and the urban area

mappings from the Third National Inventory (MCTI, 2015) for 1994, 2002, and 2010. Each selected pathway was then buffered by approximately 100 meters to define urban candidate areas.

Next, an exploratory classification was conducted using normalized difference indices for vegetation (NDVI) and water (NDWI) to mask out vegetated and aquatic regions (**Figure 4**).

The final urban mask was derived from the intersection of the filtered OpenStreetMap-based mask and the results from the exploratory classification (**Figure 5** and **Figure 6**). The non-urban mask was defined as the symmetrical difference of this final urban mask.

Random points were then generated within the search area of each of the 522 tiles. These points were labeled as urban or non-urban using PostGIS, based on the final masks (**Figure 7**), resulting in a labeled dataset of training samples for the years 1985, 1994, 2002, 2010, and 2018.

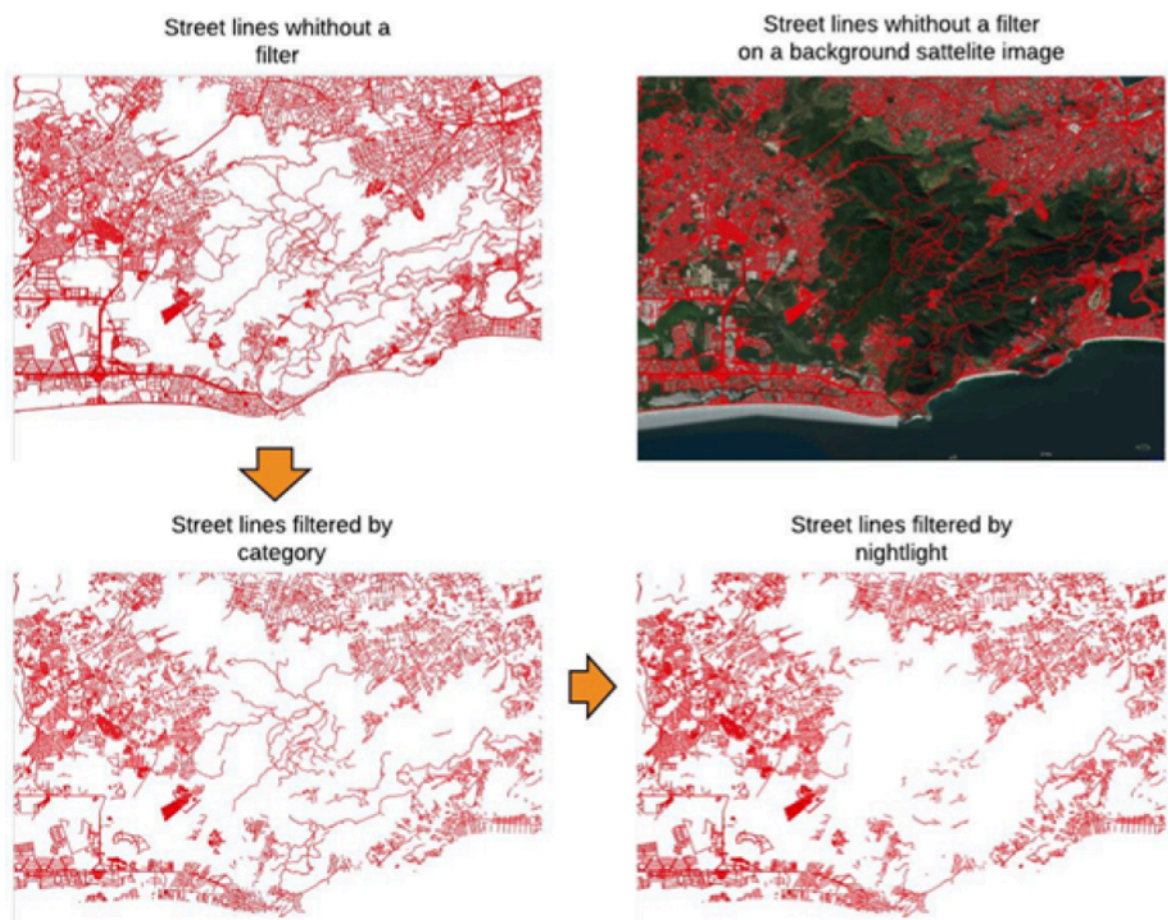


Figure 3. Example of filters used on the vector layer of OpenstreetMap in Rio de Janeiro - RJ Brazil.



Figure 4. Exploratory classification results for Rio de Janeiro - RJ, Brazil.



Figure 5. Final urban mask for Rio de Janeiro - RJ, Brazil.



Figure 6. Final non urban mask (orange color) for Rio de Janeiro - RJ, Brazil.

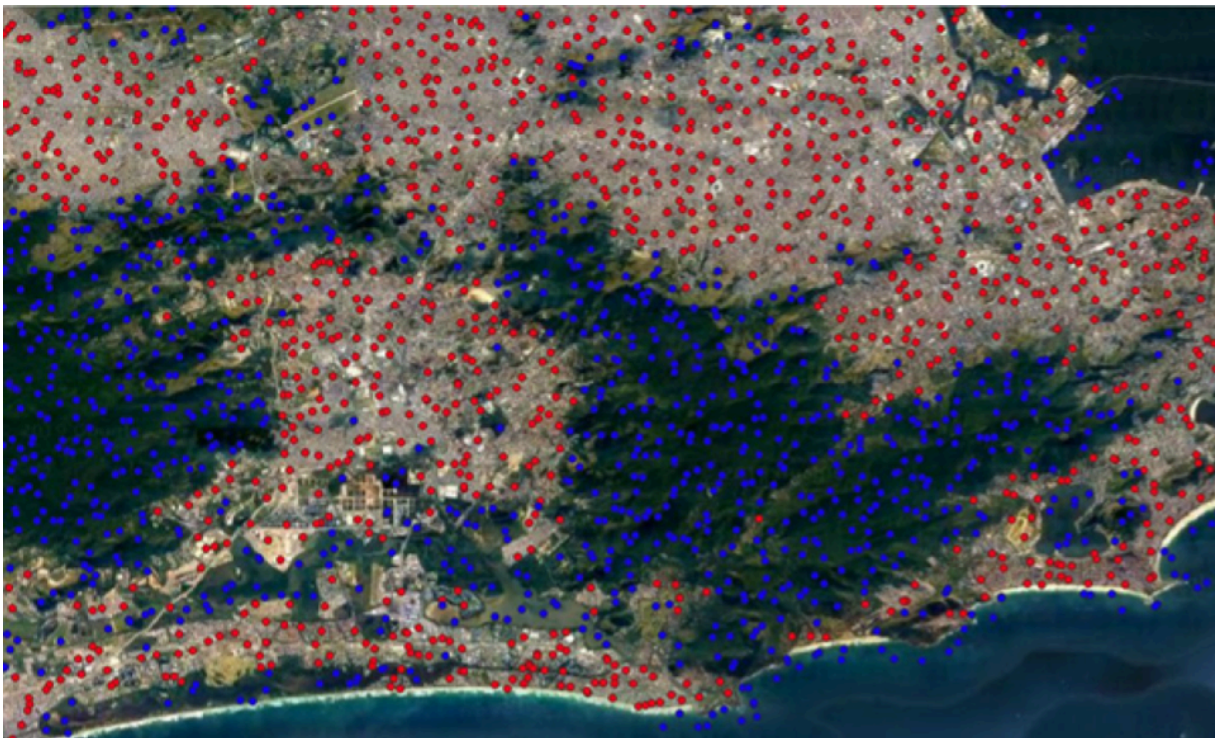


Figure 7. Random points divided by urban areas (red) and non-urban areas (blue).

This method enabled the automatic generation of a large and comprehensive sample dataset, totaling 891,427 non-urban and 532,520 urban samples for 1985; 883,101 non-urban and 453,857 urban samples for 1994; 977,644 non-urban and 546,407 urban samples for 2010; and 971,507 non-urban and 614,208 urban samples for 2018.

3.3. Classification algorithm

The Random Forest algorithm implemented in Google Earth Engine (`smileRandomForest`) was applied to map urban areas in MapBiomas Collection 10.0 using training samples of urban and non-urban areas. Random Forest parameters were set to 120 trees and 5 minimum leaf populations. In the Random Forest algorithm, the output mode was set to probability, resulting in a classification image assigning to each pixel its probability of being urban.

Sequential steps were followed to optimize the classification parameters Google Earth Engine. Based on a sub-set of the processing units covering Brazilian capitals (a total of 65 tiles; see Section [Spatial scope](#)), sample selection and mosaic refinement were conducted. For that, the years of 1985, 1990, 2000, 2010 e 2020 were used. For each year and unit, different sample quantities (see section [Samples selection](#)) and mosaic compositions (see section [Feature Space](#)) were analyzed through a Random Forest classification (see section [Random Forest training and classification](#)) with a view to define adequate parameters to be used for the entire Brazilian territory and temporal series. These parameters were assumed as the sample's quantities and mosaic composition with best classification performance.

Both sample selection and mosaic refinement were guided by the Receiver Operating Characteristic (ROC) curve and the Area Under the Curve (AUC) metric (Bradley, 1997; Fawcett, 2006). The ROC curve is a graphical representation used to evaluate the performance of binary classification models. It plots the True Positive Rate (TPR) against the False Positive Rate (FPR) across various threshold values (equations 1 and 2, respectively), allowing assessment of the model's ability to discriminate between urban and non-urban areas. The AUC summarizes this performance into a single value: the closer it is to 1, the better the model is at distinguishing between the two classes.

$$\text{TPR} = \text{TP} / (\text{TP} + \text{FN}) \quad \text{Eq. 1}$$

$$\text{FPR} = \text{FP} / (\text{FP} + \text{TN}) \quad \text{Eq. 2}$$

Where:

TP = True Positives (urban correctly classified)

FP = False Positives (non-urban wrongly classified as urban)

FN = False Negatives (urban wrongly classified as non-urban)

TN = True Negatives (non-urban correctly classified)

After defining sample quantities and mosaic composition, a Random Forest classification was applied considering the whole time series to generate annual urban classification probabilities for each processing grid. These results were subsequently harmonized temporarily (from 1985 to 2024, annually, see section [Temporal smoothing](#)), and a cutoff threshold was estimated per grid to produce a binary classification of urban areas (see section [Urban areas binary classification](#)).

3.3.1. *Samples selection*

Sample selection refers to the process of determining the optimal number of urban and non-urban samples required for effective classification. The optimal quantity was defined as the point beyond which increases in sample size did not yield significant improvements in classification accuracy. Based on experimental tests, a range of 30 to 300 randomly selected urban samples was evaluated iteratively using a standard mosaic (see supplementary table **ST3**). A fixed class balance of 1:2 (urban to non-urban samples) was adopted, based on prior results.

To calculate the ROC curve, AUC, and additional accuracy metrics for each sample size, a separate validation set of 400 urban and 800 non-urban samples (also randomly selected) was used.

Considering the results (see supplementary figure **SF. 1**), the selected urban samples quantity to classify each processing grid were 220 units. Further details of the classification process are provided in the section [Random Forest training and classification](#).

3.3.2. *Feature Space*

To support urban classification, several mosaic compositions were evaluated using predefined sets of Landsat bands, spectral indices, and spectral mixture components. Each mosaic set was tested to identify the most effective combination for classification purposes (see supplementary table **ST4** for details of each configuration). The evaluated mosaics included the following list and their combination:

- Bands - Composed of the original Landsat spectral bands from the Surface Reflectance collection.
- Indices 1 - Comprising basic indices related to vegetation, water, soil, and urban areas, calculated from Landsat Surface Reflectance data.
- Indices 2 - Included indices derived from thermal band, using Landsat Raw data.
- Mix 1 - Spectral mixture bands obtained from Spectral Mixture Analysis (SMA) (see table **ST2** and **ST4**).
- Mix 2 - Additional spectral mixture bands (see table **ST2** and **ST4**).
- Bands used in MapBiomass Collection 9 - complete mosaic as defined in supplementary table **ST1** complemented with the Automated Water Extraction Index (AWEIsh) and the Soil Adjusted Vegetation Index (SAVI).

The results show that the model performed well even for simpler mosaics (see supplementary figure **SF. 2**). A mosaic similar to what was used in Collection 9 was selected for consistency with previous MapBiomass collections. Therefore, the feature space selected to characterize Urban Areas for MapBiomass Collection 10.0 is the dataset of urban and non-urban points trained with the complete mosaic, with no differences from the one used for urban areas of Collection 9 of MapBiomass (see the example of **Figure 8**).

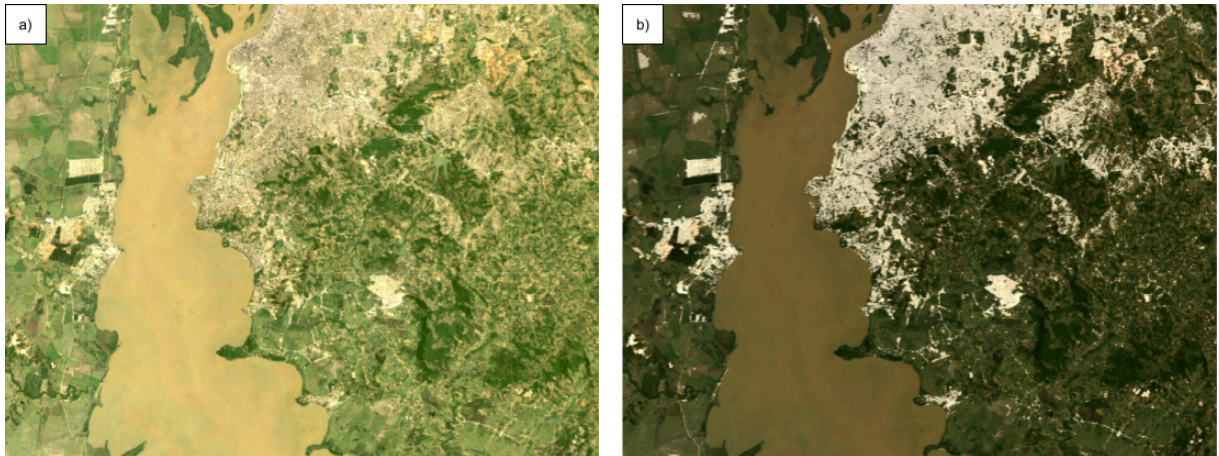


Figure 8. Classification example using the selected mosaic. Porto Alegre - RS, Brazil.

a) Landsat mosaic. b) Classification probability overlaid with the mosaic - The white areas are the most probable to be urban.

Samples selection was used with the assumption that once a point was urban, it remained urban for the following years. Therefore, images of 1985 up to 1993 were used to train the dataset of 1985, resulting in one feature space per year per tile. Likewise, images of 1994 up to 2002 were used to train the dataset of 1994, images of 2003 up to 2009, to train the dataset of 2003, images of 2010 up to 2017, to train the dataset of 2010 and images of 2018 up to 2023, to train the dataset of 2018.

3.3.3. *Random Forest training and classification*

The following Random Forest classification procedures were applied to support sample selection, mosaic refinement, and binary classification of urban areas. First, samples were based on the processing grid (see Section [Spatial scope](#)). To ensure a diverse spectral representation and optimize sample availability, the training area for each grid unit was defined as its surrounding neighborhood intersecting the previously defined search area. Within this area, a subset of available samples was randomly selected for training.

The model training was implemented using a moving window approach: a block of nine grid units (3×3) was used, where the central unit served as the classification target, and the nine neighboring units provided the training data (**Figure 9**). For evaluation purposes, the final validation was conducted using MapBiomass validation samples (see [MapBiomass website](#)).

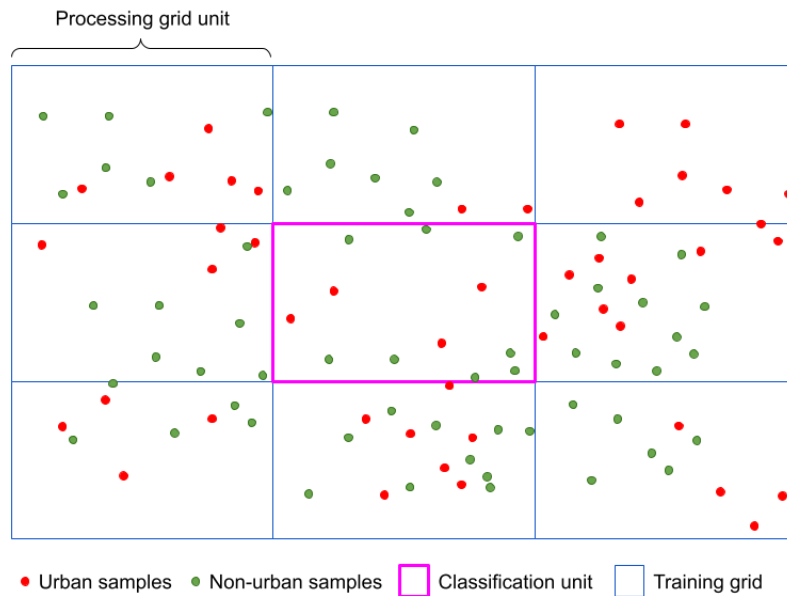


Figure 9. Processing grid for classification scheme.

3.3.4. Temporal smoothing

Following classification using the selected samples and mosaic configuration, the probability results were temporally smoothed. This was done by calculating the mean urban classification probability over five-year intervals throughout the entire time series. The procedure aimed to enhance temporal consistency while simplifying post-classification processes. An example illustrating the impact of this approach is presented in **Figure 10**.

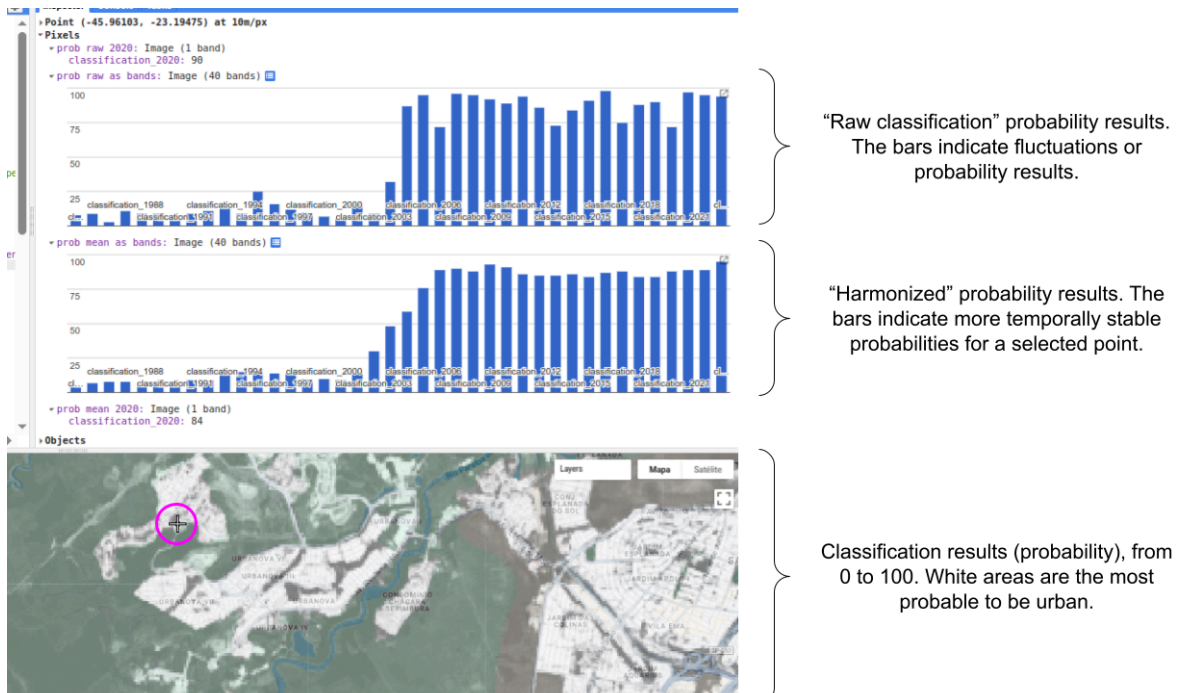


Figure 10. Example of temporal harmonization impact. São José dos Campos - SP, Brazil.

3.3.5. Urban areas binary classification

To produce the final binary classification of urban areas, a thresholding strategy based on ROC curve analysis and probability distributions of urban samples was implemented. For each processing grid unit and year, the optimal classification threshold was estimated by calculating the ROC curve and evaluating the classification probabilities associated with urban reference samples. After comparing the results, the value corresponding to the 15th percentile of urban sample probabilities was selected as the cutoff for binary classification. The only exception was the case of Corumbá municipality, an isolated urban area within the Pantanal biome where the cutoff probability value was adopted as 50%. This iterative procedure was applied across all grid units and time steps. The final threshold value used for each grid was computed as the mean cutoff value derived from the time series, ensuring temporal consistency in the classification. This threshold value was then applied to the probability smoothed results, finally providing a binary classification of urban areas (Figure 11).

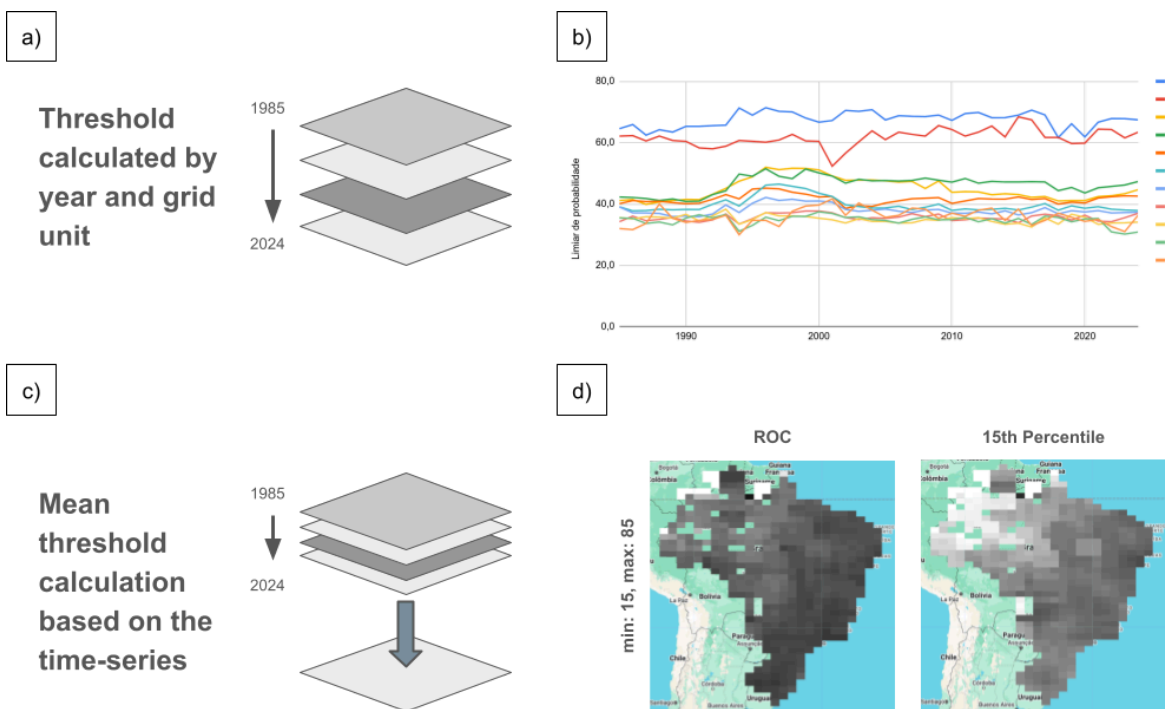


Figure 11. Summary of binary classification procedures.

a) Threshold calculation based on ROC curve and percentiles of urban classification gathered from urban samples not used during the classification. b) Example of temporal variation of cut-off values for horizontal sets of grids (covering same latitudes). c) Calculation of mean thresholds (both for ROC and selected percentile) by grid unit based on time-series results. d) Final cut-off values for each approach.

4. Post-classification procedures

Post-classification procedures were developed to improve urban area classification by addressing the inherent noise in the temporal remote sensing data, the limitations imposed by the 30-meter Landsat spatial resolution, and common confusions among land cover types and urban areas (Herold; Liu; Clarke, 2003; Lu; Weng, 2007). These procedures also accounted for the typical patterns of urban and settlement configurations in Brazil. The final output is a binary raster distinguishing urban from non-urban areas.

4.1. Gap fill

A gap-filling procedure (Figure 12) was applied to correct no-data pixels—originating from cloud and cloud shadow masking—by replacing them with the most frequent (mode) class value from neighboring years within a 3-year temporal window (one year previous the year in analysis, and two years forward). Assuming classification quality improves toward recent years, this filtering is applied backward through time. For boundary years (1985, 2023 and 2024), the window was adapted to include all available years, keeping the window size: for 1985, the years 1986, 1987 and 1988 were used; for 2023, the years 2021, 2022 and 2024, and for 2024, the years 2021, 2022 and 2023 were used to fill no-data values and maintain temporal consistency.

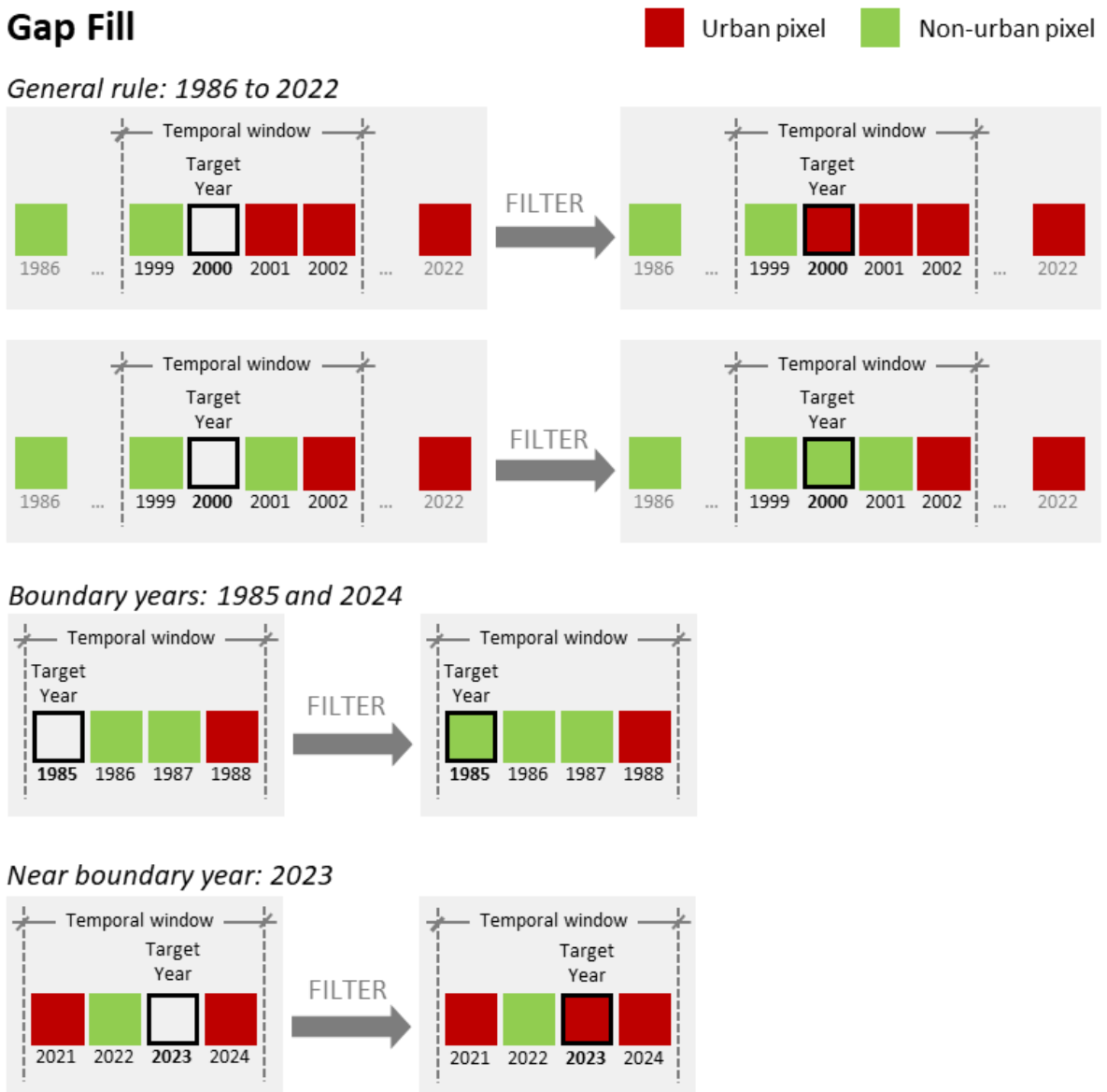


Figure 12. Gap-filling procedure.

4.2. Temporal filter

Pixels in the time series can exhibit one of three behaviors: a unique transition from non-urban to urban, stable urban status throughout, or stable non-urban status throughout. The temporal filter is designed to preserve these patterns with minimal interference, ensuring that transitions are singular and stable states are consistently maintained over time.

To operationalize this objective, the following steps were taken:

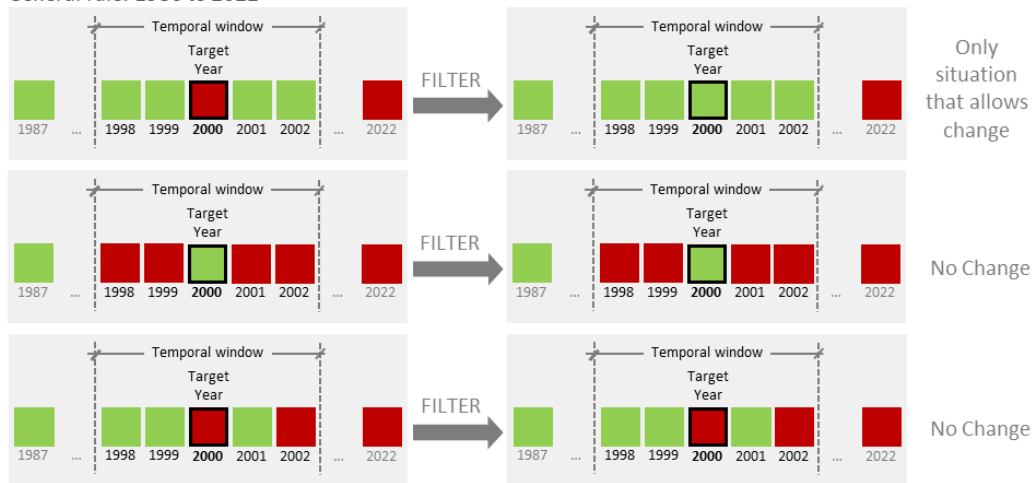
(i) Eliminate isolated urban pixels (Figure 13), i.e. pixels with values differing from their neighbors within a 5-year window (function TempFilter_wMask_5yearsunique): Unique urban pixel values are identified within a 5-year window centered on the target year. If the target year's value differs from the majority of the surrounding years, it is corrected to match the majority. Following the same assumption and logic applied in the gap-filling procedure, this filter is applied backward through time. For boundary year (1985) and near boundary years (1986, 2023), the 5-year window is adjusted to include all available neighboring years. The year of 2024 will remain unchanged in all cases.

Temporal Filter

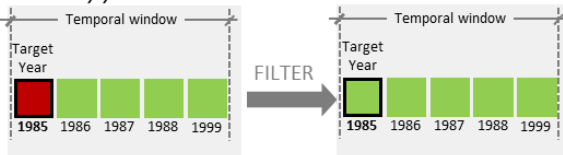
(i) Isolated urban pixel

Urban pixel Non-urban pixel

General rule: 1986 to 2022



Boundary years: 1985



Near boundary years: 1986 or 2023

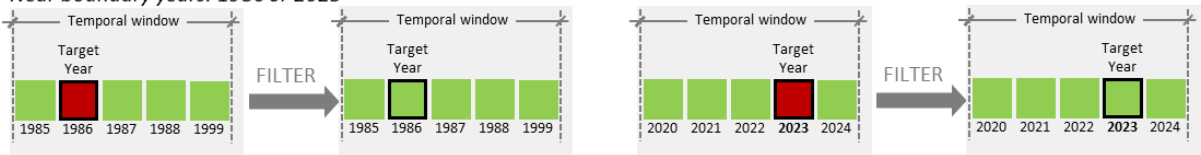


Figure 13. Temporal filter: isolated urban pixel.

(ii) Identify breakpoints (function `getBreakpoints`) (Figure 14): For each year, a pixel is classified as breakpoints if it: (1) exhibits a valid transition from non-urban to urban in that year; (2) remains urban for at least half of the remaining years in the time series; and (3) its urban persistence is higher than one, i.e. it is urban for at least one subsequent year.

- Valid transitions (function `getTransitions_valid`) are detected by comparing classifications between consecutive years (the target year and the previous year). Pixels that change from non-urban to urban are marked as valid transitions, assessed annually from 1986 to 2024. Pixels classified as urban in 1985 are assumed to originate from a valid transition.
- Urban persistence is calculated by pixel, for each year, consisting in the number of subsequent years - including the target year - during which the pixel remains classified as urban (function `getUrbToEnd`).

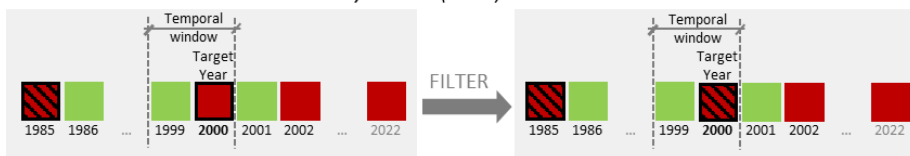
Temporal Filter

(ii) Break point identification

Urban pixel Non-urban pixel Valid transition

Valid transition identification

General rule: 1986 to 2024 and First year rule (1985)



Valid transition: change from non-urban to urban.

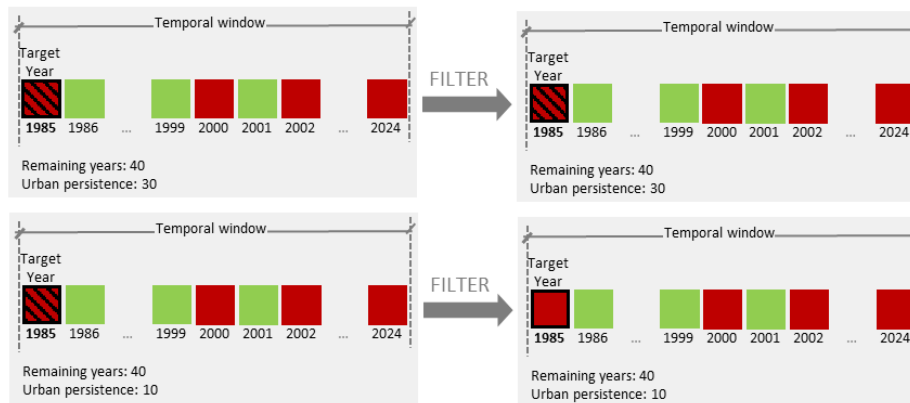
Special case (1985): pixels classified as urban in 1985 are assumed to result from a valid transition.

Valid transition confirmation

General rule: 1985 to 2024

Remaining years: number of years from the target year to 2024 (inclusive)

Urban persistence: number of remaining years in which the pixel is classified as urban



Transition remains valid if urban persistence $\geq 50\%$.

Figure 14. Temporal filter: break point identification.

(iii) Select the first breakpoint and accumulate forward (function `accumulateForward`) (Figure 15): This final step iterates, for each pixel, through the time-ordered list of breakpoints to identify the first occurrence of a breakpoint. From this point onward, the pixel is consistently classified as urban for all subsequent years, ensuring temporal consistency after the initial transition.

Temporal Filter

(iii) Break Point Selection and Forward Urban Accumulation

General rule: 1985 to 2024

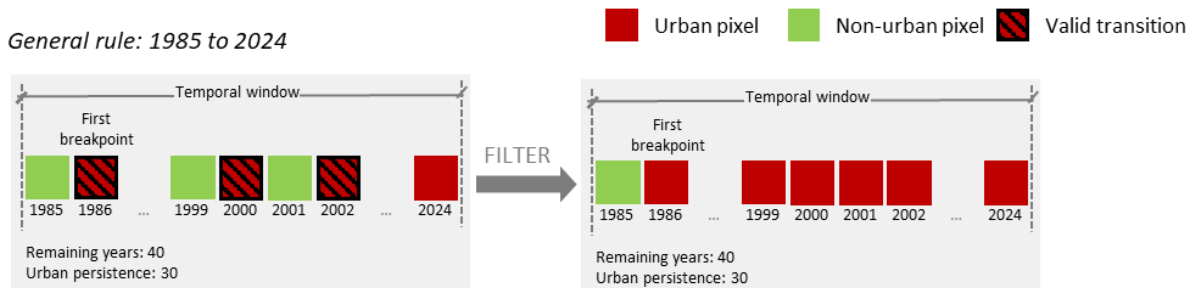


Figure 15. Temporal filter: break point selection and forward urban accumulation.

This combination of steps ensures that breakpoints represent sustained and meaningful urbanization events rather than noise or transient changes.

4.3. Spatial filter

The spatial filter was developed to reduce commission errors by applying a spatial mask to exclude areas unlikely to be urban, and to improve spatial coherence by eliminating small holes within urban areas and scattered, sparse settlements.

To build the spatial mask, high-resolution ancillary datasets were used, including:

- Index of Roads and Infrastructure v2 (IRS) (Justiniano *et al.*, 2022): The IRS defines urban limits according to roads and infrastructure density, derived from Open Street Maps datasets, used with a threshold of greater than or equal to 500.
- Urban areas (IBGE, 2022): This is the reference data for urban areas in Brazil, and was obtained through visual interpretation of Sentinel-2/MSI imagery (10m of spatial resolution for year 2019), supplemented by higher-resolution data where necessary. For the spatial mask, all urban classes—including high-density and low-density urban areas, and vacant urbanized areas—were included. Polygons classified as “other urban equipment,” which typically correspond to areas characterized exclusively by non-residential establishments, were excluded.
- Google Open Buildings v3 (Sirko *et al.*, 2021): Building footprints inferred in May 2023 from high-resolution (50 cm) satellite imagery. Building polygons with confidence $\geq 65\%$ were buffered by 25 meters to better capture the surrounding built-up environment and rasterized to match the 30-meter resolution of MapBiomass data. Small internal holes (≤ 5 connected pixels) were filled, and small isolated clusters (≤ 22 connected pixels) were removed to reduce noise and enhance spatial coherence.
- Favelas and urban communities (IBGE, 2020): This dataset, which serves as a basis for the most recent Demographic Census of Brazil, was used to complement the other datasets, particularly in regions that were underrepresented due to spatial resolution or other limitations of the previous datasets.

All ancillary datasets were converted into binary raster and combined using an inclusive rule: a pixel is included in the spatial mask if it is identified as urban in at least one of these datasets. This spatial mask was then applied sequentially to the temporal filter for each year,

excluding areas classified as urban that are likely commission errors—such as bare soil within agricultural fields and rocky outcrops.

The final post-classification step applies filters based on connected pixel counts. For urban holes, a threshold of 280 pixels (approximately 25 hectares) was used, according to IBGE’s definition of vacant urban spaces (IBGE, 2022). Areas smaller than this threshold are, therefore, incorporated into the urban final classification.

Conversely, urban noise, defined as isolated small clusters of urban pixels, was reclassified as non-urban. An empirical threshold of 44 pixels (approximately 4 hectares) was applied. These clusters typically correspond to non-urban structures, such as agricultural buildings, infrastructure, or transportation facilities and were removed.

The final product of these procedures is a set of annual raster datasets, spanning from 1985 to 2024, mapping urban areas across the Brazilian territory. This dataset was integrated with other thematic maps to compose MapBiomass Collection 10 Land Cover and Land Use.

5. Comparison with previous collections

For each MapBiomass collection, the classification methodology is updated and the entire time series is reprocessed, resulting in a recalculation of the mapped class areas. As a result, variations in the total mapped urbanized area are expected between collections, as illustrated in **Figure 12**. For Collection 10, the total mapped urbanized area starts at approximately 1.80 million hectares in 1985 and increases over time, reaching around 4.55 million hectares by 2024.

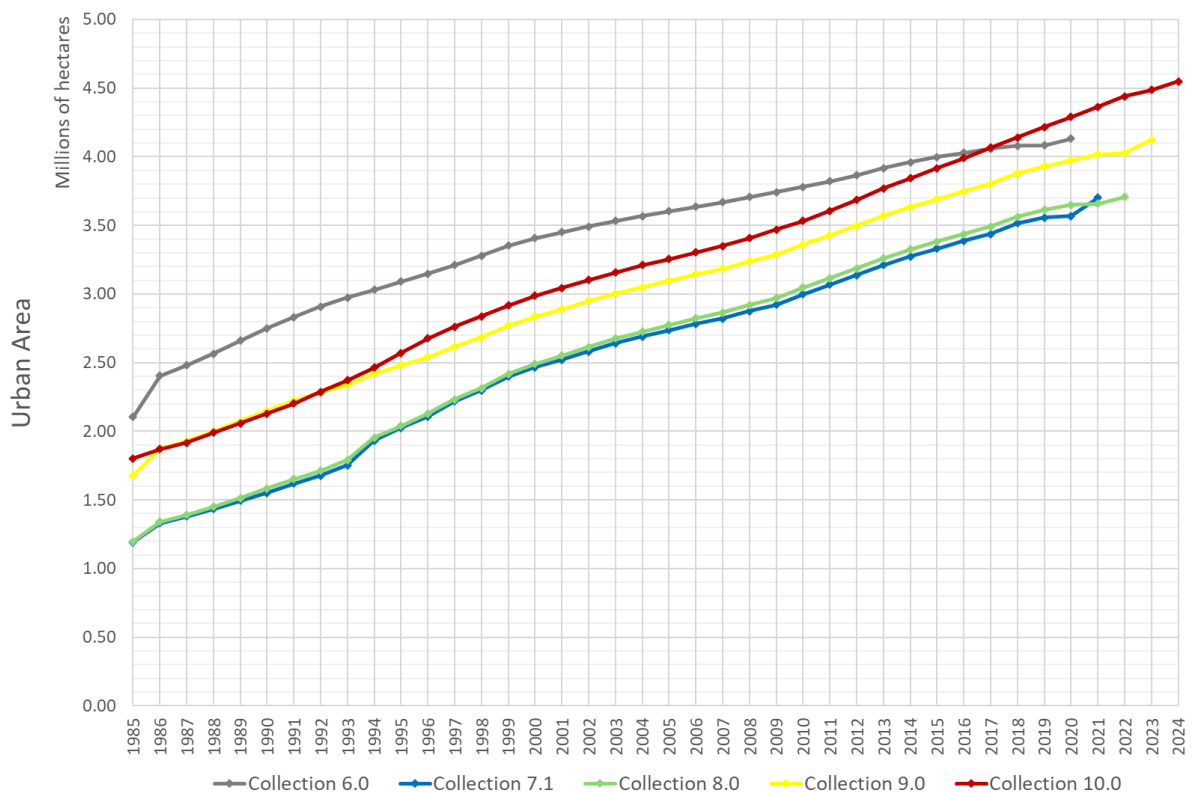


Figure 16. Total urban area (in millions of hectares) mapped by year in MapBiomass Collections 6, 7.1, 8, 9, and 10

Figure 16 represents differences between collections, reflecting the evolution of classification methodologies over time. Collection 6 stands out as the most distinct, reporting consistently higher urbanized areas throughout the time series, especially in the early years, reflecting earlier classification methods that tended to overestimate urban areas compared to subsequent collections. Collections 7.1 and 8 display very similar trajectories throughout the time series, especially in the early years, which aligns with their methodological similarity. Collections 9 and 10 also follow closely aligned trends in the initial period (1985–1994), but begin to diverge after 1994, with Collection 10 detecting systematically larger urbanized areas, particularly in more recent years. It is worth noting that the sharp increase from 1985 to 1986 observed in all previous collections was corrected in Collection 10, which shows a smoother and more gradual transition between these years.

A qualitative comparison between Collections 9 and 10 highlights clear improvements in spatial detail. As shown in Figure 10, Collection 10 presents a more refined delineation of urban areas, particularly along the urban-rural interface. Compared to Collection 9, Collection 10 more accurately captures the built-up footprint, reducing commission errors in adjacent vegetated areas (**Figure 17 [A]** and **[B]**). Notably, it also better identifies linear urbanization patterns, such as small settlements along roadways, which appear more fragmented or underrepresented in Collection 9 (**Figure 17 [C]** and **[D]**).

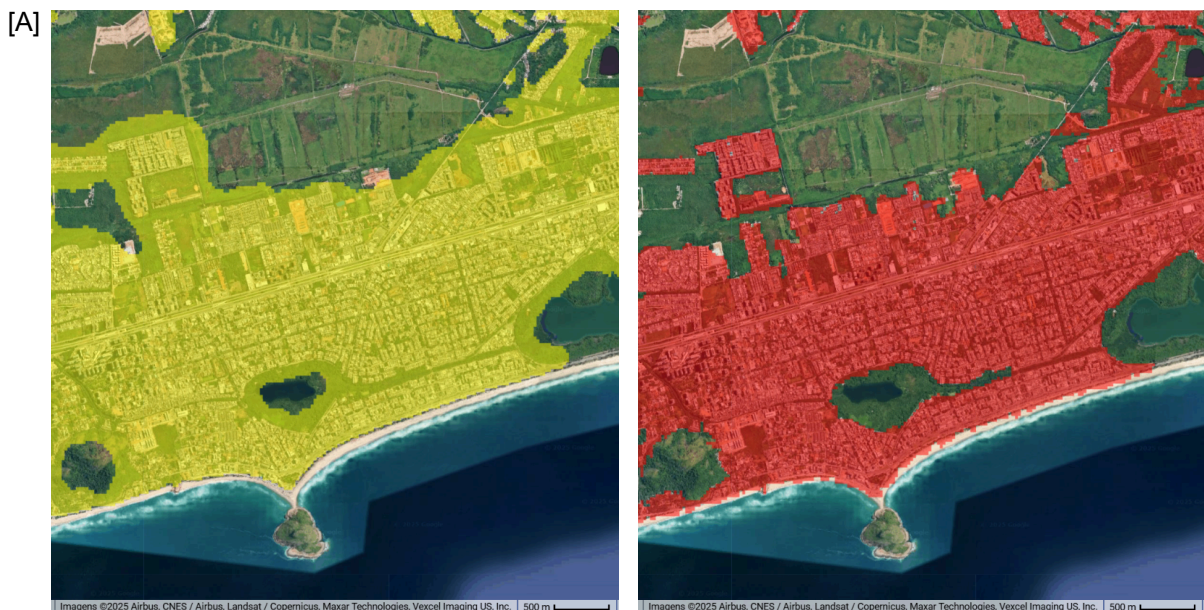




Figure 17. Comparison of urban area mapping between Collections 9 and 10 in two locations: [A] Rio de Janeiro (RJ) and [B] Agudo (RS). In each location, yellow represents the urban area mapped in Collection 9, and red represents Collection 10.

6. Validation Strategies

6.1. Accuracy Analysis

Following MapBiomass LULC validation strategy, the error assessment analysis was conducted using ~75,000 samples per year, labeled according to MapBiomass LULC classes by experts after the visual interpretation of Landsat data, MODIS-NDVI times series, and high-resolution imagery from Google Earth (when available). The accuracy analysis was based on Stehman (Stehman, 2014; Stehman; Foody, 2019) using the population error matrix and the global, user, and producer accuracies.

The accuracy results are published on the MapBiomass website² and are reproduced here for the Urban Area class in **Figure 18** (Producer's Accuracy) and **Figure 19** (User's Accuracy).

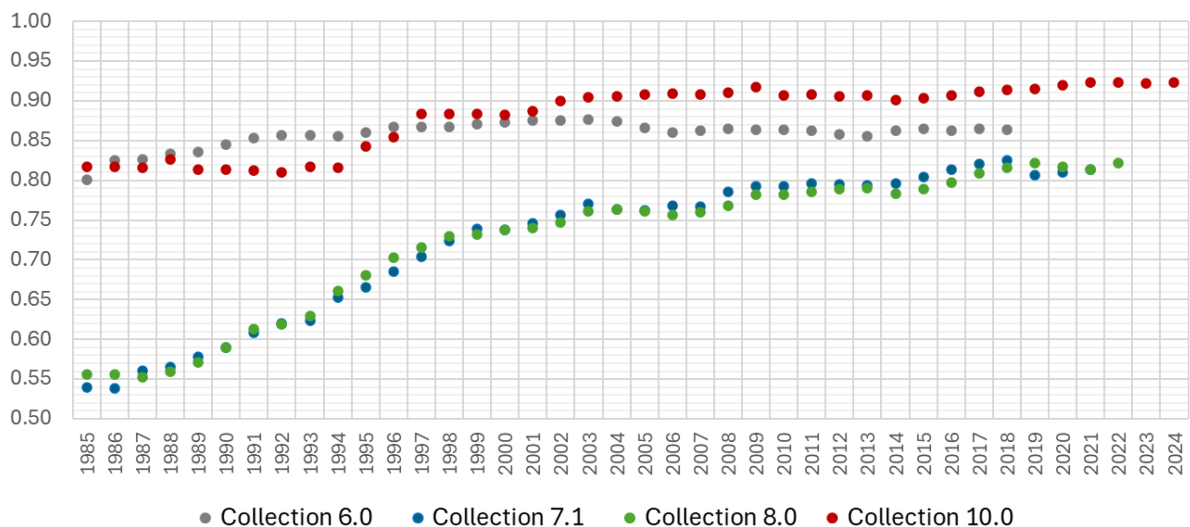


Figure 18. Producer's accuracy

² <https://brasil.mapbiomas.org/en/estatistica-de-acuracia/colecao-10/>

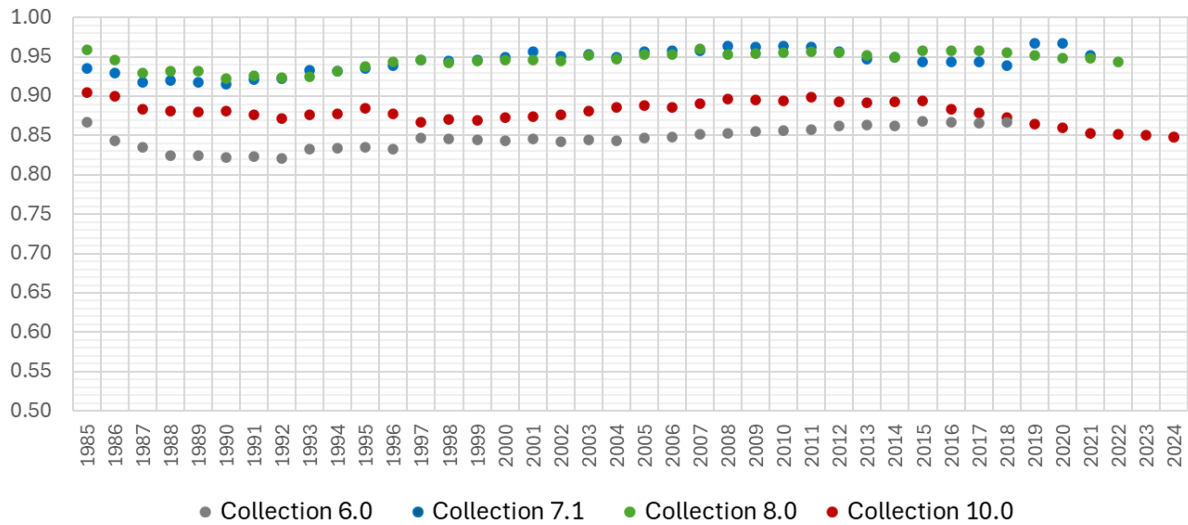


Figure 19. User's accuracy

In terms of Producer's Accuracy, Collection 10 consistently shows the highest values across all years, especially from 2000 onwards, maintaining levels above 90%. This reflects a significant improvement in minimizing omission errors, meaning urban areas are more completely captured compared to earlier collections. For User's Accuracy, Collection 10 also shows consistently high performance but with a slight decreasing trend in recent years. It maintains values generally above 85%, which indicates good reliability in minimizing commission errors (i.e., reducing the inclusion of non-urban areas as urban). However, the highest User's Accuracy in the early years (1985–2000) is observed in Collections 7.1 and 8.0, likely due to their more conservative mapping approach. From 2000 onwards, Collection 10 remains stable, balancing a higher Producer's Accuracy with good User's Accuracy.

Overall, Collection 10 outperforms previous collections in terms of Producer's Accuracy while maintaining competitive User's Accuracy, demonstrating the effects of methodological improvements aimed at reducing omission errors without excessively increasing commission errors.

6.2. Comparison with reference maps

MapBiomas Collection 10.0 were compared to two urban area maps: (1) the World Settlement Footprint (WSF) produced by Deutsches Zentrum für Luftund Raumfahrt (DLR) (Marconcini *et al.*, 2020) and (2) Brazil Urbanized Areas produced by IBGE, Instituto Brasileiro de Geografia e Estatística (IBGE, 2022).

WSF is a 10m resolution binary mask outlining the extent of human settlements globally derived by means of 2014-2015 multitemporal Landsat-8 and Sentinel-1 imagery, using different classification schemes based on Support Vector Machines. It is available at Earth Engine Data Catalog³.

Quantitative analysis (**Table 1**) indicates that the urbanized area mapped in 2015 by MapBiomas Collection 10.0 totals 3,916,797 hectares, surpassing the 3,421,975 hectares mapped by the World Settlement Footprint (WSF). The area mapped exclusively by

³ https://developers.google.com/earth-engine/datasets/catalog/DLR_WSF_WSF2015_v1

MapBiomass amounts to 1,051,152 hectares, while WSF uniquely maps 556,329 hectares. Despite these differences, both datasets share a concordant area of 2,865,645 hectares. Overall, the overlap between MapBiomass and WSF reaches 83.7% across the Brazilian territory. When disaggregated by biome, the Pantanal exhibits the lowest overlap (73.5%), while all other biomes show overlaps exceeding 80%.

Table 1. Comparison of Urban Area Mapping between MapBiomass Collection 10 and the World Settlement Footprint -WSF (Marconcini et al., 2020) for the Year 2015.

Year: 2015	Total Area Mapped by Col. 10 (in ha)	Total Area Mapped by WSF (in ha)	Area Only Mapped by Col. 10 (in ha)	Area Only Mapped by WSF (in ha)	Overlapping Area (in ha)	Overlap Relative to WSF (in %)
Amazon	377,062	314,743	116,752	54,433	260,310	82.7%
Caatinga	521,692	337,433	243,478	59,219	278,214	82.5%
Cerrado	882,059	737,625	262,030	117,596	620,029	84.1%
Atlantic Forest	1,997,877	1,898,665	404,553	305,341	1,593,324	83.9%
Pampa	133,893	128,935	23,485	18,527	110,408	85.6%
Pantanal	4,213	4,572	854	1,214	3,359	73.5%
Brazil	3,916,797	3,421,975	1,051,152	556,329	2,865,645	83.7%

Brazil Urbanized Areas is a visual interpretation of urban features, identified according to the elements of specific shape (geometry of objects) and pattern (spatial arrangement), using Sentinel 2 imagery, with spatial resolution of 10m, supplemented by higher-resolution data where necessary. It is available in shapefile format at IBGE's website⁴. The mapped urban land use types include: "Urbanized Area," categorized into two classes — high density and low density —, "Other Urban Facilities," and "Vacant Urbanized Areas."

The comparison with IBGE's 2019 data points to an underestimation of MapBiomass Collection 10.0 urban area (**Table 2**). For the year 2019, the urbanized area mapped by Collection 10 totals 4,215,208 hectares, while the Urbanized Areas dataset identifies a larger extent of 5,321,060 hectares. The area mapped exclusively by Collection 10 amounts to 475,366 hectares, whereas Urbanized Areas exclusively accounts for 1,581,219 hectares. The overlapping area between the two datasets reaches 3,739,841 hectares. Considering the entire Brazilian territory, this represents a 70.3% overlap relative to the total mapped by Urbanized Areas. When analyzed by biome, the overlap varies, with the Cerrado (75.4%) and Atlantic Forest (70.9%) exhibiting the highest levels of agreement, while the Amazon (65.3%) and Caatinga (64.1%) show lower concordance. The Pantanal displays a moderate overlap of 69.4%, and the Pampa reaches 69.7%.

4

<https://www.ibge.gov.br/geociencias/cartas-e-mapas/redes-geograficas/15789-areas-urbanizadas.html?=&t=acesso-ao-produto>

Table 2. Comparison of Urban Area Mapping between MapBiomias Collection 10 and the Urbanized Areas (IBGE, 2022) for the Year 2019.

Year: 2019	Total Area Mapped by Collection 10	Total Area Mapped by Urbanized Areas	Area Only Mapped by Collection 10	Area Only Mapped by Urbanized Areas	Overlapping Area	Overlap Relative to Urbanized Areas
Biome	(in ha)	(in ha)	(in ha)	(in ha)	(in ha)	(in %)
Amazon	402,349	567,544	31,828	197,023	370,521	65.3%
Caatinga	594,173	716,514	134,666	257,007	459,507	64.1%
Cerrado	950,399	1,101,385	119,443	270,428	830,956	75.4%
Atlantic Forest	2,124,634	2,738,989	182,877	797,231	1,941,758	70.9%
Pampa	139,229	190,538	6,355	57,664	132,874	69.7%
Pantanal	4,423	6,091	198	1,866	4,225	69.4%
Brazil	4,215,208	5,321,060	475,366	1,581,219	3,739,841	70.3%

7. Urban Module

The Urban Module of the MapBiomias platform provides a comprehensive mapping of urbanized areas in Brazil from 1985 to 2024, based on Collection 10 data. It offers access to urbanization data by year and in 5-year intervals, as well as information on urban vegetation and urbanization patterns relative to slope and elevation from the nearest drainage. The methodology used to generate each of the module’s layers is detailed in the following sections.

7.1. Urban Vegetation

The urban vegetation layer provides a detailed breakdown of the class Urban Area (ID=24), which, according to the definition adopted here, also includes open areas containing vegetation. Thus, the legend of the urban vegetation layer presents, at the first level, the “Urban Area” class, which is further detailed into vegetated urban areas, corresponding to vegetation in squares, parks, and public and private areas, and non-vegetated areas, which are built-up or paved areas.

The urban vegetation layer also includes non-urban areas entirely contained within the urban extent, represented by a first-level legend class termed “Non-urban Area.” These areas, referred to as urban vacant areas (voids), consist of large remnants of natural vegetation or unoccupied land exceeding 25 ha. They are further classified into forest, herbaceous and shrubby vegetation, farmland, non-vegetated areas, and water.

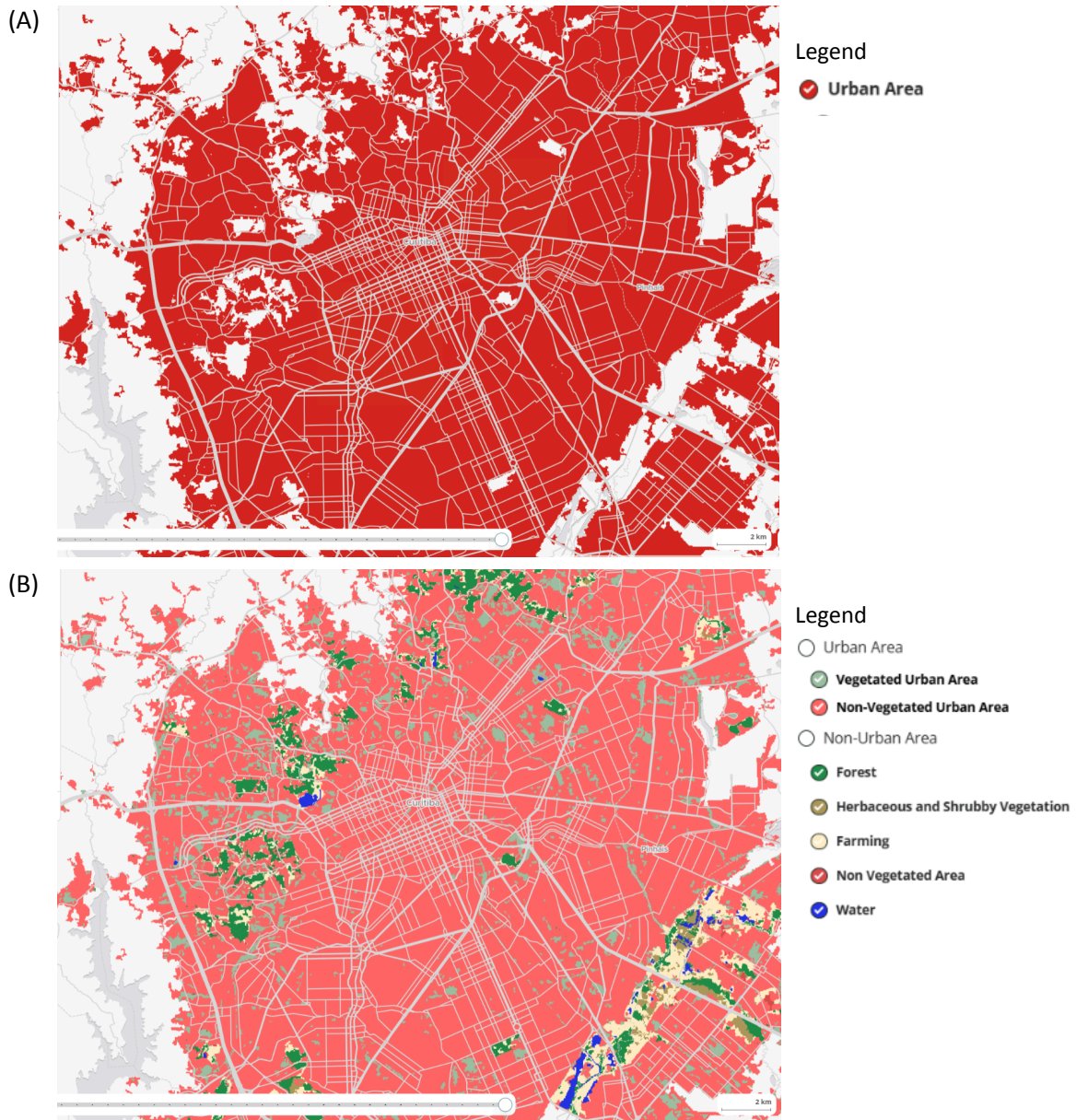


Figure 20. City of Curitiba in 2024, showing: (A) Urban Areas (ID=24) in the Land Use and Land Cover data, Collection 10, and (B) urban vegetation layer data, with legend levels 1 and 2.

The methodology for deriving the urban vegetation layer was based on Collection 10 land use and land cover maps, encompassing all mapped classes. The workflow comprises four main steps: (1) mapping of vacant urban spaces; (2) generation of preliminary urban vegetation map; (3) application of spatial and temporal filters; and (4) compilation of the final urban vegetation layer. The following sections provide a detailed description of these procedures, followed by the results and validation of the intra-urban vegetation data.

7.1.1. Procedures

7.1.1.1. Vacant urban spaces (voids) map

To map vacant urban spaces, the following steps were performed:

- a) Annual images from Collection 10 were binarized into Urban Area and Non-Urban Area classes;
- b) Each urban area patch was subsequently vectorized;
- c) A union overlay was applied between each urban patch and its corresponding bounding box;
- d) From this union, polygons that satisfied both of the following conditions were retained as vacant urban spaces (voids): (i) no spatial intersection with the urban patch (i.e., disjoint geometries); and (ii) no topological contact with the bounding box boundary;
- e) These vectors were then used as masks and applied to the Collection 10 Land Use and Land Cover maps to generate the urban voids image dataset.

7.1.1.2. Preliminary Urban Vegetation Map

The probability data generated as described in item 3 of this document (Subitems 3.1, 3.2, 3.3.1, 3.3.2, and 3.3.3) were used to separate non-vegetated from vegetated urban areas. Initially, this dataset was masked using the binarized Collection 10 data so that probability values were considered only within areas mapped as Urban Areas (ID = 24) in the final Collection 10 product. Subsequently, a 50% threshold was applied to distinguish, within urbanized areas, non-vegetated areas (paved or built-up pixels) from vegetated areas.

Vegetated areas within the vacant urban spaces (voids) were then added to the vegetated areas within urban extents derived from the probability map to compose the preliminary urban vegetation map. This merging of vegetated areas is required to enable the application of temporal and spatial filters that account for the continuity of urban vegetation. The result of this step is a binary raster dataset: value 1 corresponds to urban vegetation, and value 0 corresponds to non-vegetated urban area.

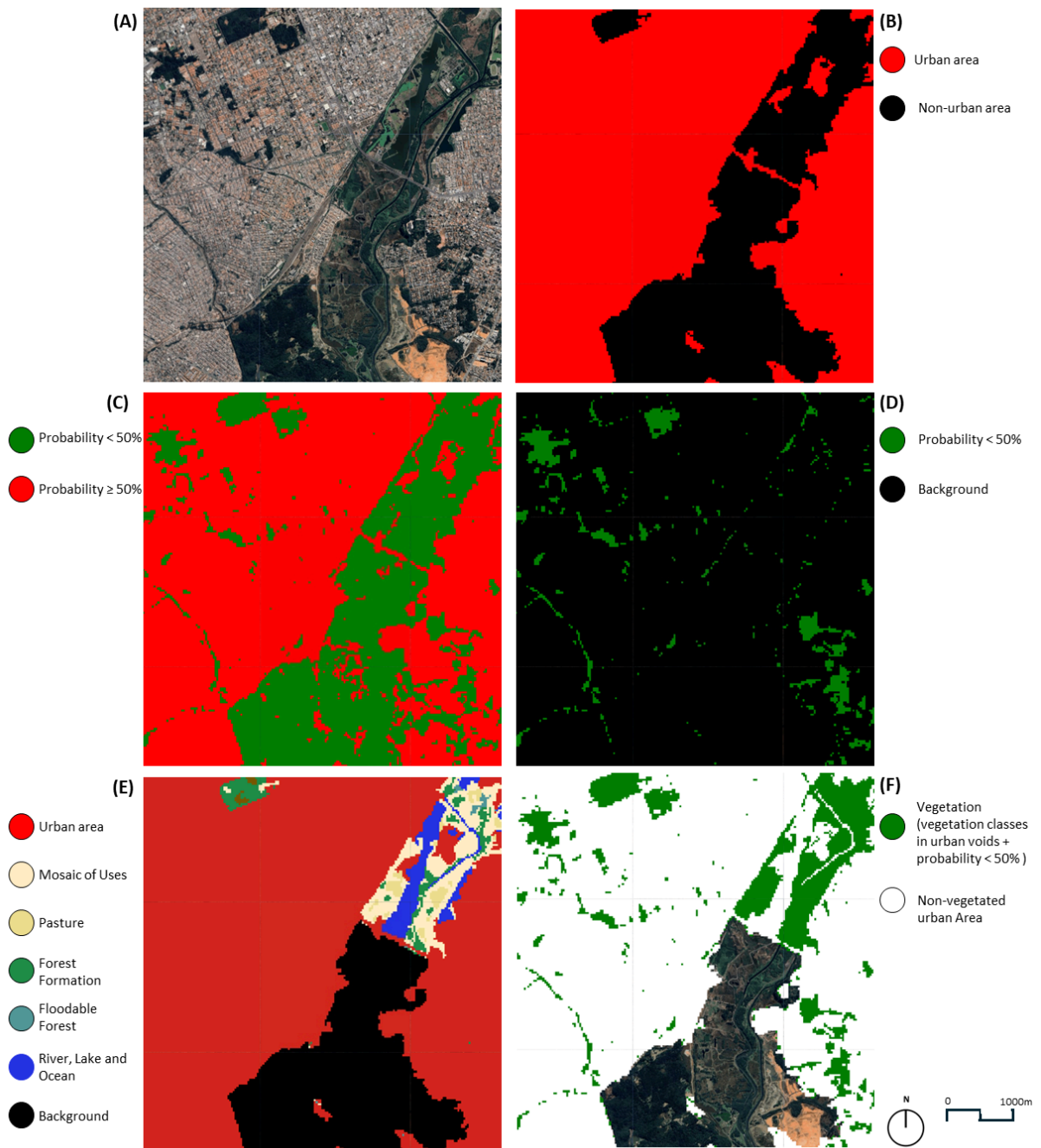


Figure 21. City of Curitiba in 2024, showing: (A) Google Satellite image, (B) Urban Area mask; (C) Probability map; (D) Probability <math>< 50\%</math> within urban area; (D) Urban Areas + Urban Vacant Area (voids) map; and (E) Preliminary Urban Vegetation map.

7.1.1.3. Temporal and spatial filters

Filters were designed to produce a conservative classification of urban vegetation, retaining only areas that are more likely to represent true vegetation. In this context, vegetated area is required to occur in patches of at least five connected pixels ($4,500\text{m}^2$) and to persist over time for five years or more.

The spatial and temporal filters to achieve this were applied as follows:

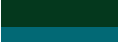
- a- Spatial Filter 1: eliminates spatially isolated pixels, both from vegetated and non-vegetated classes of the preliminary Urban Vegetation map.
- b- Temporal Filter: eliminates vegetation pixels for which the previous year and the following year were non-vegetation, or vice versa (non-vegetation pixels that were vegetation), for the years 1986 to 2023. For 1985, the first year and the two subsequent years were considered. This filter was not applied to the last year of the temporal series to retain possible transitions to vegetation.
- d- Frequency Filter: eliminates urban vegetation pixels that are not present for more than five consecutive years. Pixels in the final years (2023 or 2024) are retained even if they do not meet the full consecutive-vegetation threshold, in order to prevent edge effects and avoid an artificial end-of-series bias. The asymmetric treatment of the time-series boundaries reflects differences in observational support, with conservative filtering applied where future confirmation is available and permissive filtering applied where data truncation would otherwise bias the results.
- e- Spatial Filter 2: retains as urban vegetation only groups of five or more connected pixels.

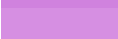
7.1.1.4. Final data assembly

In the final step, the vegetation dataset with all filters applied was masked using the Urban Area class (ID = 24) to create two subclasses within the “Urban Area” first level class: vegetated urban areas and non-vegetated urban areas.

This dataset was combined with the urban voids map to incorporate these areas into the final product while preserving their original pixel classifications. The final legend of the urban vegetation dataset is presented in Table 2.

Table 2. Complete Legend of the Urban Vegetation Layer.

<i>Level</i>	<i>Class name</i>	<i>Class ID</i>	<i>Color</i>	<i>Color Code</i>
1	Urban Area	24		#d4271e
2	Non-vegetated Urban Area	240		#ff6666
2	Vegetated Urban Area	241		#9bbfa1
1	Non-urban area	243		#6c8770
2	Forest	1		#1f8d49
3	Forest Formation	3		#1f8d49
3	Savanna Formation	4		#7dc975
3	Mangrove	5		#04381d
3	Floodable Forest	6		#026975
3	Wooded Sandbank Vegetation	49		#02d659
2	Herbaceous and Shrubby Vegetation	10		#ad975a
3	Wetland	11		#519799

<i>Level</i>	<i>Class name</i>	<i>Class ID</i>	<i>Color</i>	<i>Color Code</i>
3	Grassland	12		#d6bc74
3	Hypersaline Tidal Flat	32		#fc8114
3	Rocky Outcrop	29		#ffaa5f
3	Herbaceous Sandbank Vegetation	50		#ad5100
2	Farming	14		#ffefc3
3	Pasture	15		#edde8e
3	Agriculture	18		#E974ED
4	Temporary Crop	19		#C27BA0
5	Soybean	39		#f5b3c8
5	Sugar cane	20		#db7093
5	Rice	40		#c71585
5	Cotton (beta)	62		#ff69b4
5	Other Temporary Crops	41		#f54ca9
4	Perennial Crop	36		#d082de
5	Coffee	46		#d68fe2
5	Citrus	47		#9932cc
5	Palm Oil	35		#9065d0
5	Other Perennial Crops	48		#e6ccff
3	Tree Plantation	9		#7a5900
3	Mosaic of Uses	21		#ffefc3
2	Non vegetated area	22		#db4d4f
3	Beach, Dune and Sand Spot	23		#ffa07a
3	Mining	30		#9c0027
3	Photovoltaic Power Plant (beta)	75		#c12100
3	Other non-Vegetated Areas	25		#db4d4f
2	Water	26		#2532e4
3	River, Lake and Ocean	33		#2532e4
3	Aquaculture	31		#091077

7.1.2. Results

The Vegetation dataset was produced using a conservative approach to ensure that all mapped vegetation represents true vegetation. Accordingly, to be classified as vegetated urban area, a patch must cover at least five connected pixels (4,500 m²) and persist for a minimum of five years.

From 1985 to 2024, a steady increase was observed in total urban area and urban vacant area (urban voids), driven primarily by the expansion of non-vegetated (built-up) urban land, which remains the dominant component throughout the period (Figure 23). Vegetated urban areas also increase consistently, indicating that green spaces within cities have expanded alongside urban growth rather than being entirely replaced. In addition, vegetation in non-urban areas (urban voids) shows a gradual upward trend, although it contributes a much smaller share compared to urban land uses.

In 1985, cities contained about 158,000 ha of vegetated urban area, increasing nearly fourfold to around 620,000 ha by 2024, indicating substantial growth in urban green spaces

over time. Remnants of vegetation within urban voids also expanded, rising from 56,000 ha in 1985 to almost 150,000 ha in 2024.

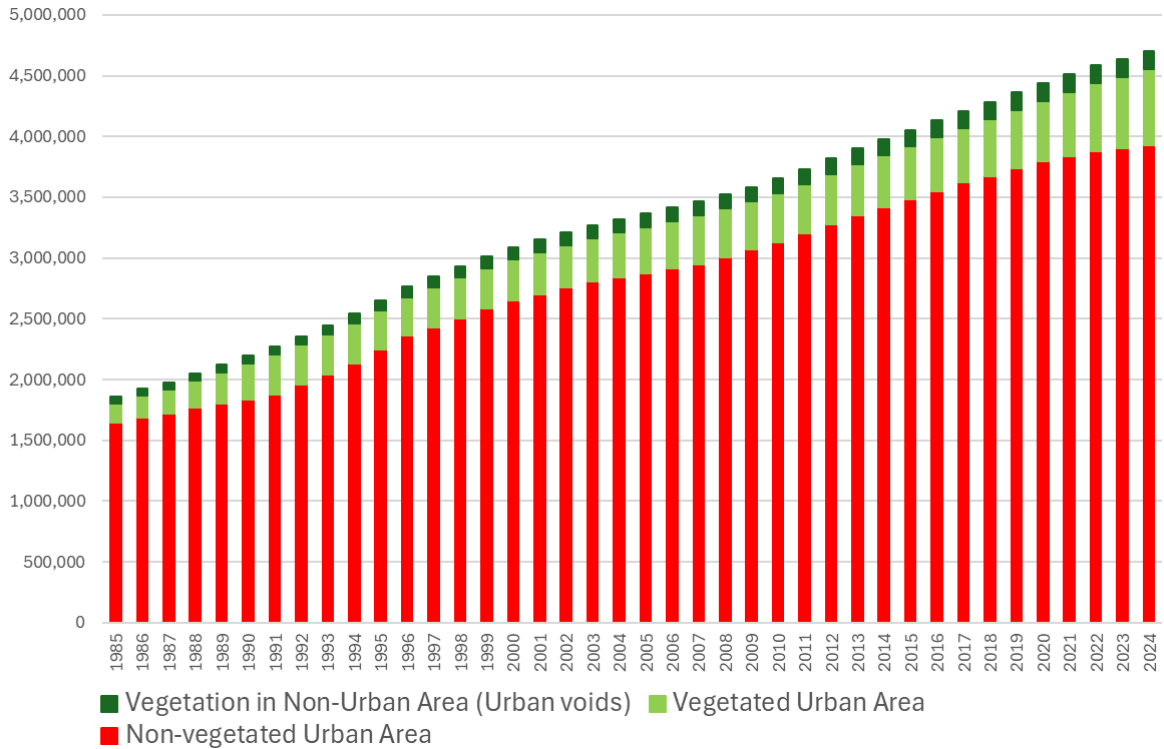


Figure 23. Vegetated and Non-Vegetated Urban Areas (1985–2024) in Brazil.

To calculate the total vegetation in urban areas and urban voids, the Urban Vegetation dataset was reclassified into vegetated and non-vegetated categories based on the Level 2 legend classes, as presented in Table 3. The same reclassification categories were consistently applied to the more detailed levels (3 to 5) according to the Level 2 scheme.

Table 3. Reclassification of the Urban Vegetation Dataset into Vegetated and Non-Vegetated Categories Based on Level 2 Legend Classes.

<i>Class name (Level 1)</i>	<i>Class name (Level 2)</i>	<i>Reclass</i>
Urban Area	Non-vegetated Urban Area	Non-vegetated area
	Vegetated Urban Area	Vegetated area
Non-urban area	Forest	Vegetated area
	Herbaceous and Shrubby Vegetation	Vegetated area
	Farming	Vegetated area
	Non vegetated area	Non-vegetated area
	Water	Not considered

Results indicate that, between 1985 and 2024, the total vegetated area within urban areas and urban voids increased from around 214,000 ha to about 770,000 ha, rising from 11.5% to 16.4% of the total. During the same period, non-vegetated areas grew from around 1,650,000 ha to about 3,940,000 ha. In relative terms, non-vegetated areas were 7.7 times larger than vegetated areas at the beginning of the series, but this ratio declined to 5.1 by the

end, suggesting that although built-up land continued to grow, vegetated areas increased at a faster rate, as presented in Figure 20.

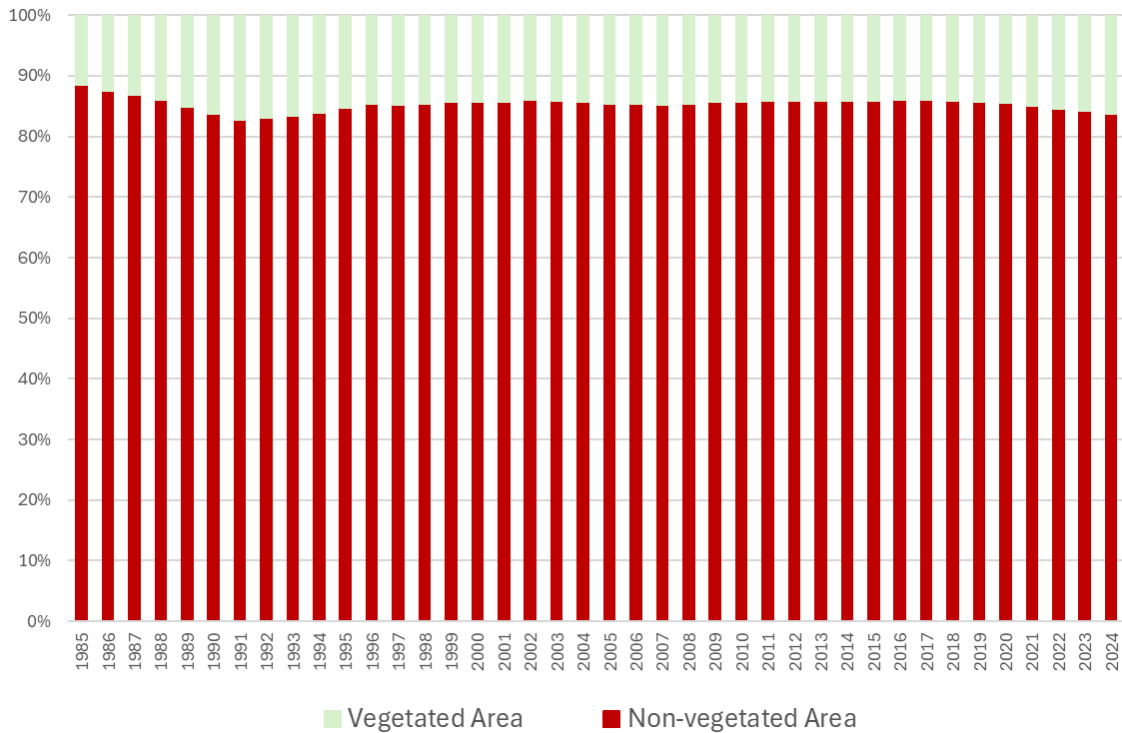


Figure 21. Proportional Distribution of Vegetated and Non-Vegetated Urban Areas in Brazil (1985-2024).

The increase in urban vegetation results from two processes: the creation of new green areas within cities, and the expansion of urban areas, which incorporate surrounding peri-urban vegetation. Once incorporated, these areas may either be progressively built over or, in some cases, remain as vacant / undeveloped areas (Figure 24).

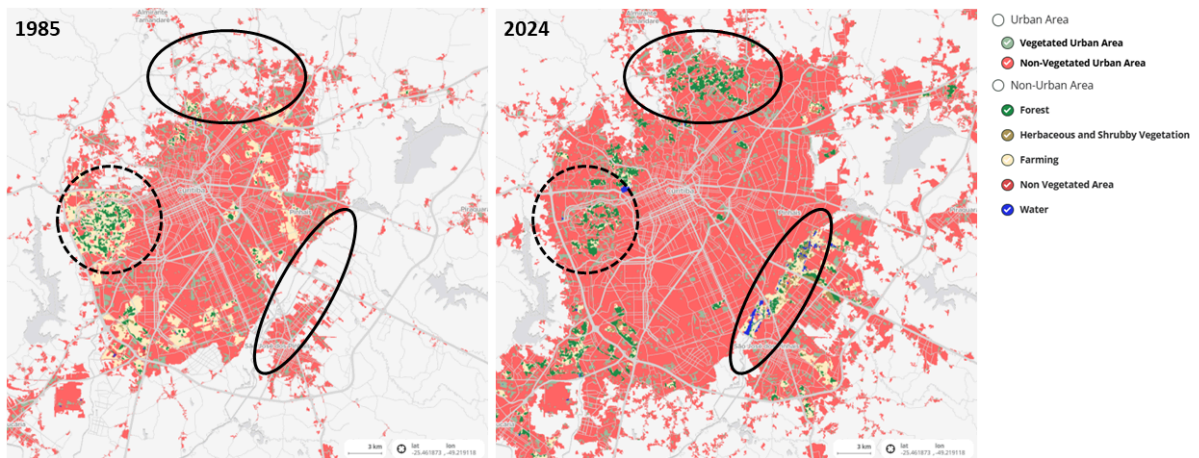


Figure 24. Processes of vegetation incorporation and loss during the urban growth of Curitiba between 1985 and 2024. Dashed areas indicate the loss of vegetation fragments, while solid-line areas show the incorporation of peri-urban vegetation into the urban fabric.

However, when excluding the effects of urban expansion into peri-urban areas, a decline in urban vegetation is observed. Using the urbanized area in 1985 (1.8 million hectares) as a mask, the proportion of remaining vegetation decreases from 11.5% to 8.8%, highlighting the ongoing conversion of vegetated areas into built-up surfaces (Figure 25).

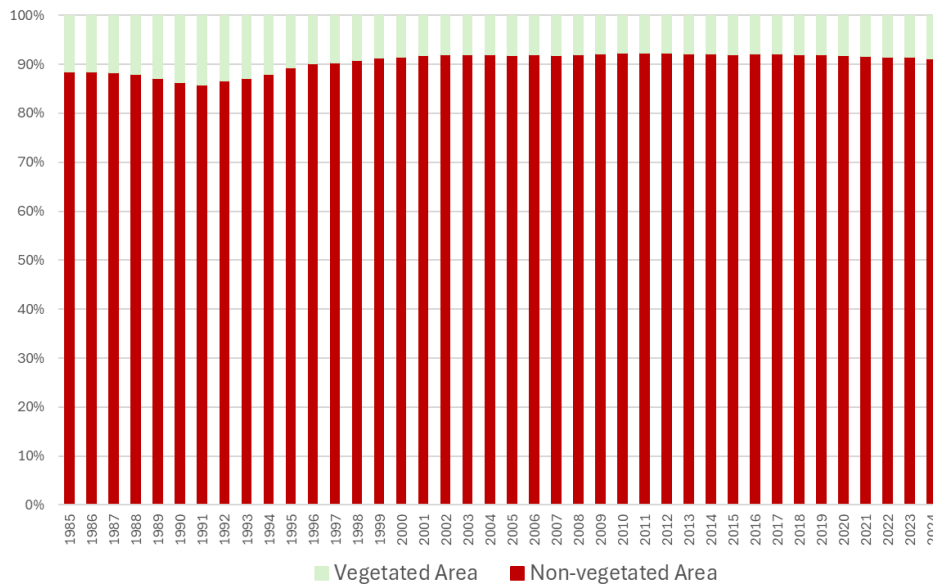


Figure 25. Decline of urban vegetation in Brazilian cities, relative to the 1985 urbanized area (1.8 million ha), showing the progressive conversion of vegetation into built-up areas between 1985 and 2024.

7.1.3. Comparison with other datasets

The urban vegetation data from MapBiomias Collection 10 was compared to the Digital Vegetation Cover Map of São Paulo (2020), produced by the Municipality of São Paulo (PMSP)⁵. This data was created by integrating high-resolution aerial imagery and LiDAR data to capture detailed vegetation structure across the entire municipality, with the reference year being 2017. The dataset report indicates 7,359,900 ha of vegetation in the municipality, representing 48,18% of the total municipal area.

For comparison with MapBiomias data, the PMSP dataset was resampled to the same 30 m resolution as MapBiomias, and only vegetation patches larger than 4,500 m² and located within the urban area or urban void were considered. Using these criteria, urban vegetation in São Paulo totals 14,900 ha.

Applying the reclassification scheme described in Table 3, the MapBiomias dataset was grouped into vegetated and non-vegetated areas for comparison with the PMSP dataset.

As shown in Table 4, the MapBiomias dataset mapped 10,979 ha of vegetation, while 77,075 ha of non-vegetated area were consistently identified in both datasets. Areas mapped

⁵ Digital Vegetation Cover Map of São Paulo report is available at [https://drive.prefeitura.sp.gov.br/cidade/secretarias/upload/meio_ambiente/RelCobVeg2020_vFINAL_compressed\(1\).pdf](https://drive.prefeitura.sp.gov.br/cidade/secretarias/upload/meio_ambiente/RelCobVeg2020_vFINAL_compressed(1).pdf)

as vegetated only in MapBiomas correspond to 1,989 ha, whereas areas mapped only in the PMSP dataset total 5,910 ha. Vegetated areas identified in both datasets amount to 8,990 ha, indicating substantial overlap but also highlighting differences in detection between the datasets.

Table 4. Comparison of Urban Vegetation Between PMSP and MapBiomas Collection 10 datasets.

Vegetation (30 m resolution, >4,500 m² patches) in 2017	Area (hectares)
Total vegetated area PMSP dataset	14,900
Total vegetated area MapBiomas dataset	10,979
Non-vegetated area mapped in both datasets	77,075
Vegetated area mapped only in MapBiomas's dataset	1,989
Vegetated area mapped only in PMSP's dataset	5,910
Vegetated area mapped in both datasets	8,990

Assuming the PMSP dataset as the reference ground truth, the overall accuracy obtained for the MapBiomas dataset is 91.6%, with a producer's accuracy for vegetated areas of 60.3% and a consumer's accuracy of 81.9%, indicating that the MapBiomas dataset tends to under-detect vegetated areas rather than falsely classifying non-vegetated areas as vegetation.

Urban vegetation estimates from both datasets were calculated for each administrative district of São Paulo to enable a district-level comparison (Figure 26). The regression slope below one (0.8591) and the negative intercept suggest a systematic underestimation of urban vegetation by MapBiomas relative to the PMSP reference, particularly in districts with larger vegetated areas. This pattern is consistent with the omission detected in the producer's accuracy. A strong linear relationship ($R^2 = 0.9563$) was observed, indicating high overall spatial consistency across all districts. Despite some underestimation of vegetation area, this R^2 indicates that the dataset is sufficiently reliable for comparative analyses between areas and cities.

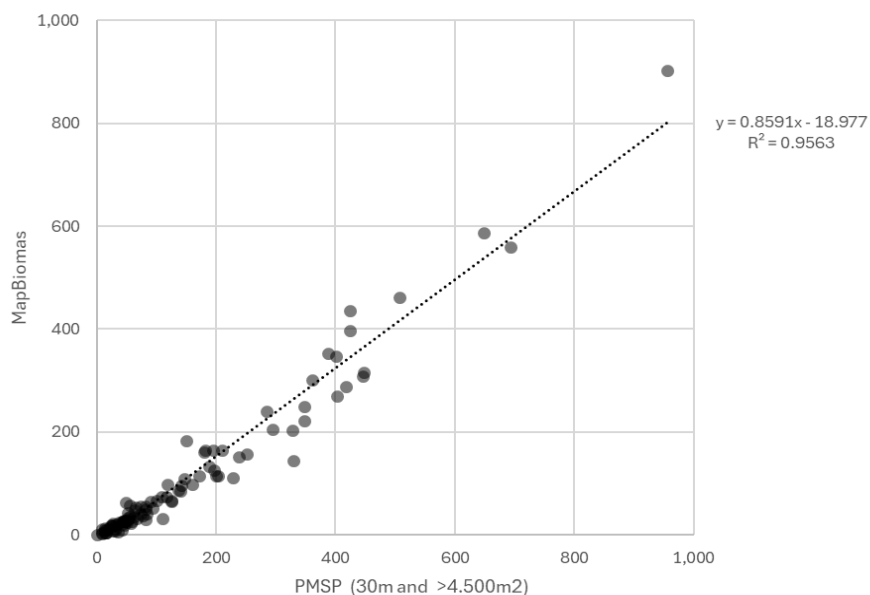


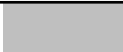
Figure 26. Comparison of urban vegetation area by district between datasets (2017). Each dot represents a district.

7.2. Urbanization periods

The Urbanization Periods layer depicts the spatial and temporal dynamics of urban expansion in Brazil from 1985 to 2024 derived from the MapBiomas Collection 10 land-use and land-cover time series and aggregated into 5-year intervals.

For each year (1985–2024), pixels classified as “Urban Area” (ID = 24) were extracted and assigned a temporary value corresponding to the year of observation. These annual layers were combined into a multi-band image, and a pixel-wise minimum was computed to identify the earliest year each pixel was urbanized. The resulting raster was then reclassified into 5-year periods, producing a single-band image where each value represents the urbanization period of that pixel, according to Table 5.

Table 5. Complete Legend of the Urbanization Periods Layer.

<i>Level</i>	<i>Class name</i>	<i>Class ID</i>	<i>Color</i>	<i>Color Code</i>
1	Urbanized up to 1985	1		#bfbfbf
1	Urbanized between 1986 and 1990	2		#c0afc8
1	Urbanized between 1991 and 1995	3		#a8a9db
1	Urbanized between 1996 and 2000	4		#9f8ed2
1	Urbanized between 2001 and 2005	5		#7d7ed3
1	Urbanized between 2005 and 2010	6		#7a6fc9
1	Urbanized between 2011 and 2015	7		#b05ea6
1	Urbanized between 2016 and 2020	8		#b73875
1	Urbanized between 2021 and 2024	9		#930000

7.3. Urban Slope

The Urban Slope layer depicts the topographic characteristics of urban areas in Brazil derived from digital elevation model (DEM), classified into four slope categories according to Table 6. The DEM used was the NASA 30m Digital Elevation Model (NASA, 2020), available directly on GEE.

For each pixel classified as "Urban Area" (ID = 24) in the MapBiomas Collection 10 land-use and land-cover product, slope values were extracted from a digital elevation model and classified into four categories based on percentage inclination. The resulting raster represents the predominant slope class of each urban pixel, according to Table 6.

Table 6. Complete Legend of the Urban Slope Layer.

<i>Level</i>	<i>Class name</i>	<i>Class ID</i>	<i>Color</i>	<i>Color Code</i>
1	Slope ≤ 10%	132		#ffc6a8
1	Slope between 10% and 20%	133		#ff7a34
1	Slope between 20% and 30%	134		#e63b22
1	Slope > 30%	135		#8c1a14

7.4. Height above nearest drainage

The HAND (Height Above Nearest Drainage) layer depicts the relative elevation of urban areas in Brazil in relation to the nearest drainage network, classified into three categories according to Table 7. A globally available HAND model (Donchyts et al. 2016), originally generated with an accumulation threshold of 100 cells and available directly on GEE, was employed.

For each pixel classified as "Urban Area" (ID = 24) in the MapBiomass Collection 10 land-use and land-cover product, HAND values were extracted and classified into three categories. The resulting raster represents the HAND class of each urban pixel, according to Table 7.

Table 7. Complete Legend of the Urban HAND Layer.

<i>Level</i>	<i>Class name</i>	<i>Class ID</i>	<i>Color</i>	<i>Color Code</i>
1	HAND ≤ 3 m	142		#9cc8f2
1	3 < HAND ≤ 6 m	143		#41ab5d
1	HAND > 6 m	144		#d9b26f

8. References

AS-SYAKUR, Abd Rahman *et al.* Enhanced Built-Up and Bareness Index (EBBI) for Mapping Built-Up and Bare Land in an Urban Area. **Remote Sensing**, v. 4, n. 10, p. 2957–2970, 2012.

BRADLEY, Andrew P. The use of the area under the ROC curve in the evaluation of machine learning algorithms. **Pattern Recognition**, v. 30, n. 7, p. 1145–1159, 1997.

BREIMAN, L. Random forests. **Machine learning**, v. 45, n. 1, p. 5-32, 2001.

CORBANE, Christina *et al.* GHS-BUILT R2018A - GHS built-up grid, derived from Landsat, multitemporal (1975-1990-2000-2014). 2018. Available at: <http://data.europa.eu/89h/jrc-ghsl-10007>.

DONCHYTS, G. et al. Global 30m Height Above the Nearest Drainage. 19 Apr. 2016. Available at: <http://dx.doi.org/10.13140/RG.2.1.3956.8880>

FAWCETT, Tom. An introduction to ROC analysis. **Pattern Recognition Letters**, v. 27, n. 8, ROC Analysis in Pattern Recognition, p. 861–874, 2006.

FEYISA, Gudina L. *et al.* Automated Water Extraction Index: A new technique for surface water mapping using Landsat imagery. **Remote Sensing of Environment**, v. 140, p. 23–35, 2014.

GAO, Bo-cai. NDWI—A normalized difference water index for remote sensing of vegetation liquid water from space. **Remote Sensing of Environment**, v. 58, n. 3, p. 257–266, 1996.

HEROLD, Martin; LIU, XiaoHang; CLARKE, Keith C. Spatial Metrics and Image Texture for Mapping Urban Land Use. **Photogrammetric Engineering & Remote Sensing**, v. 69, n. 9, p. 991–1001, 2003.

HUETE, A.R. A soil-adjusted vegetation index (SAVI). **Remote Sensing of Environment**, v. 25, n. 3, p. 295–309, 1988.

HUETE, A *et al.* Overview of the radiometric and biophysical performance of the MODIS vegetation indices. **Remote Sensing of Environment**, v. 83, n. 1, The Moderate Resolution Imaging Spectroradiometer (MODIS): a new generation of Land Surface Monitoring, p. 195–213, 2002.

IBGE. Censo Demográfico 2010 – Aglomerados Subnormais. Rio de Janeiro, RJ: IBGE, 2020.

IBGE, Coordenação de Meio Ambiente (org.). **Áreas urbanizadas do Brasil: 2019**. Rio de Janeiro, RJ: IBGE, 2022.

IBGE. **Malha de Setores Censitários**. Brasil: 2020. Malha censitária.

JUSTINIANO, Eduardo Felix *et al.* Proposal for an index of roads and structures for the mapping of non-vegetated urban surfaces using OSM and Sentinel-2 data. **International Journal of Applied Earth Observation and Geoinformation**, v. 109, p. 102791, 2022.

KAWAMURA, Makoto; JAYAMANNA, Sanath; TSUJIKO, Yuji. Quantitative Evaluation of Urbanization in Developing Countries Using Satellite Data. **Doboku Gakkai Ronbunshu**, v. 1997, n. 580, p. 45–54, 1997.

KEY, C. H.; BENSON, N. C. Landscape Assessment: Ground Measure of Severity, the Composite Burn Index; and Remote Sensing of Severity, the Normalized Burn Ratio. *In*: LUTES, D. C. *et al.* (org.). **FIREMON: Fire Effects Monitoring and Inventory System**. Ogden, UT: USDA Forest Service, Rocky Mountain Research Station, 2006. (Gen. Tech. Rep.).

LU, D.; WENG, Q. A survey of image classification methods and techniques for improving classification performance. **International Journal of Remote Sensing**, v. 28, n. 5, p. 823–870, 2007.

MARCONCINI, Mattia *et al.* Outlining where humans live, the World Settlement Footprint 2015. **Scientific Data**, v. 7, n. 1, p. 242, 2020.

MCFEETERS, S. K. The use of the Normalized Difference Water Index (NDWI) in the delineation of open water features. **International Journal of Remote Sensing**, v. 17, n. 7, p. 1425–1432, 1996.

MCTIC-Ministério da Ciência, Tecnologia, Inovações e Comunicações. **III National Inventory of Greenhouse Gas Emissions (LULUCF sector)**. 2015. Available at: https://www.gov.br/mcti/pt-br/acompanhe-o-mcti/sirene/publicacoes/relatorios-de-referencia-s-etorial/pdf/inventario3/rr_lulucf_mudanca_de_uso_e_floresta.pdf .

NASA JPL (2020). **NASADEM Merged DEM Global 1 arc second V001**. NASA EOSDIS Land Processes DAAC. doi:10.5067/MEaSURES/NASADEM/NASADEM_HGT.001

OSM. **OpenStreetMap (Standard)**, 2021.

RIKIMARU, A; ROY, P S; MIYATAKE, S. Tropical forest cover density mapping. **International Society for Tropical Ecology**, v. 43, n. 1, p. 39–47, 2002.

ROUSE, J. W. *et al.* Monitoring vegetation systems in the Great Plains with ERTS. **Anais [...]**. Texas: NASA NTRS, 1974. Available at: <https://ntrs.nasa.gov/citations/19740022614>.

SANTOS, Bruno Dias dos *et al.* Identifying Precarious Settlements and Urban Fabric Typologies Based on GEOBIA and Data Mining in Brazilian Amazon Cities. **Remote Sensing**, v. 14, n. 3, p. 704, 2022.

SIRKO, Wojciech *et al.* **Continental-Scale Building Detection from High Resolution Satellite Imagery**. [S. l.]: arXiv, 2021. Available at: <http://arxiv.org/abs/2107.12283>.

SMALL, Christopher; MILESI, Cristina. Multi-scale standardized spectral mixture models. **Remote Sensing of Environment**, v. 136, p. 442–454, 2013.

SOUZA, Carlos M.; ROBERTS, Dar A.; COCHRANE, Mark A. Combining spectral and spatial information to map canopy damage from selective logging and forest fires. **Remote Sensing of Environment**, v. 98, n. 2, p. 329–343, 2005.

STEHMAN, Stephen V. Estimating area and map accuracy for stratified random sampling when the strata are different from the map classes. **International Journal of Remote Sensing**, v. 35, n. 13, p. 4923–4939, 2014.

STEHMAN, Stephen V.; FOODY, Giles M. Key issues in rigorous accuracy assessment of land cover products. **Remote Sensing of Environment**, v. 231, p. 111199, 2019.

XU, Hanqiu. Modification of normalised difference water index (NDWI) to enhance open water features in remotely sensed imagery. **International Journal of Remote Sensing**, v. 27, n. 14, p. 3025–3033, 2006.

ZHA, Y.; GAO, J.; NI, S. Use of normalized difference built-up index in automatically mapping urban areas from TM imagery. **International Journal of Remote Sensing**, v. 24, n. 3, p. 583–594, 2003.

Supplemental material

ST. 1. Landsat imagery used in Urban Area mosaics within Google Earth Engine (GEE).

Landsat Mission, Sensor	Collection, Tier	Period	Level	GEE Collection ID	Bands [wavelength]
Landsat 5, TM	Collection 2, Tier 1	1984 to 2012	Surface Reflectance	LANDSAT/LT05/C02/T1_L2	SR_B1: Blue [0.45-0.52 μm] SR_B2: Green [0.52-0.60 μm] SR_B3: Red [0.63-0.69 μm] SR_B4: Near Infrared [0.77-0.90 μm] SR_B5: Shortwave Infrared 1 [1.55-1.75 μm] SR_B7: Shortwave Infrared 2 [2.08-2.35 μm]
			Raw Images	LANDSAT/LT05/C02/T1	B4: Near infrared [0.76 - 0.90 μm] B5: Shortwave infrared 1 [1.55 - 1.75 μm] B6: Thermal Infrared 1 (resampled from 60m to 30m) [10.40 - 12.50 μm]
Landsat 7, ETM+	Collection 2, Tier 1	2010 to 2016	Surface Reflectance	LANDSAT/LE07/C02/T1_L2	SR_B1: Blue [0.45-0.52 μm] SR_B2: Green [0.52-0.60 μm] SR_B3: Red [0.63-0.69 μm] SR_B4: Near Infrared [0.77-0.90 μm] SR_B5: Shortwave Infrared 1 [1.55-1.75 μm] SR_B7: Shortwave Infrared 2 [2.08-2.35 μm]
			Raw Images	LANDSAT/LE07/C02/T1	B4: Near Infrared [0.77 - 0.90 μm] B5: Shortwave Infrared 1 [1.55 - 1.75 μm] B6_VCID_1: Low-gain Thermal Infrared 1 (resampled from 60m to 30m) [10.40 - 12.50 μm]
Landsat 8, OLI / TIRS	Collection 2, Tier 1	2013 to 2024	Surface Reflectance	LANDSAT/LC08/C02/T1_L2	SR_B2: Blue [0.45 - 0.51 μm] SR_B3: Green [0.53 - 0.59 μm] SR_B4: Red [0.64 - 0.67 μm] SR_B5: Near Infrared [0.85 - 0.88 μm] SR_B6: Shortwave Infrared 1 [1.57 - 1.65 μm] SR_B7: Shortwave Infrared 2 [2.11 - 2.29 μm]
			Raw Images	LANDSAT/LC08/C02/T1	B5: Near infrared [0.85 - 0.88 μm] B6: Shortwave infrared 1 [1.57 - 1.65 μm] B10: Thermal infrared 1 (resampled from 100m to 30m) [10.60 - 11.19 μm]
Landsat 9, OLI / TIRS	Collection 2, Tier 1	2021 to 2024	Surface Reflectance	LANDSAT/LC09/C02/T1_L2	SR_B2: Blue [0.45 - 0.51 μm] SR_B3: Green [0.53 - 0.59 μm] SR_B4: Red [0.64 - 0.67 μm] SR_B5: Near Infrared [0.85 - 0.88 μm] SR_B6: Shortwave Infrared 1 [1.57 - 1.65 μm] SR_B7: Shortwave Infrared 2 [2.11 - 2.29 μm]
			Raw Images	LANDSAT/LC09/C02/T1	B5: Near infrared [0.85 - 0.88 μm] B6: Shortwave infrared 1 [1.57 - 1.65 μm] B10: Thermal infrared 1 (resampled from 100m to 30m) [10.60 - 11.19 μm]

Type	Name	Description	Equations (if applicable)	Statistics
Bands	BLUE	Blue	SR_B2 (L8/9), SR_B1 (L5/7)	Median
	GREEN	Green	SR_B3 (L8/9), SR_B2 (L5/7)	Median
	RED	Red	SR_B4 (L8/9), SR_B3 (L5/7)	Median
	NIR	Near Infrared	SR_B5 (L8/9), SR_B4 (L5/7)	Median
	SWIR1	Shortwave Infrared 1	SR_B6 (L8/9), SR_B5 (L5/7)	Median
	SWIR2	Shortwave Infrared 2	SR_B7 (L8/9), SR_B7 (L5/7)	Median
Urban and Bare Soil indices	NDBI	Normalized Difference Built-up Index (Zha; Gao; Ni, 2003)	$(SWIR1 - NIR) / (SWIR1 + NIR)$	Median
	EBBI	Enhanced Built-up and Bareness Index (As-syakur <i>et al.</i> , 2012)	$((SWIR1 - NIR) / (SWIR1 + NIR + RED))^{0.5}$	Median, p25, p75, p75-p25
	UI	Urban Index (Kawamura; Jayamanna; Tsujiko, 1997)	$(SWIR2 - NIR) / ((SWIR2 + NIR) + v1)$	Median
	NDRI	Normalized difference roof index (Santos <i>et al.</i> , 2022)	$(RED - BLUE) / (RED + BLUE)$	Median
	BAI	Bare soil area index (Santos <i>et al.</i> , 2022)	$(BLUE - NIR) / (BLUE + NIR)$	Median
	BU	Built-up Index (ZHA <i>et al.</i> , 2003)	NDBI - NDVI	Median
Vegetation indices	NDVI	Normalized Difference Vegetation Index (Rouse <i>et al.</i> , 1974)	$(NIR - RED) / (NIR + RED)$	Median
	EVI	Enhanced Vegetation Index (Huete <i>et al.</i> , 2002)	$2.5 * ((NIR - RED) / (NIR + 6 * RED - 7.5 * BLUE + 1))$	Median, p10, p90, p90-p10
	EVI2	Enhanced Vegetation Index modified	$2.5 * ((NIR - RED) / (NIR + 2.4 * RED + 1))$	Median, p10, p90, p90-p10
	SAVI*	Soil Adjusted Vegetation Index (Huete, 1988)	$((NIR - RED) / (NIR + RED + 0.5)) * 1.5$	Median
Water indices	MNDWI	Modified Normalized Difference Water Index (Xu, 2006)	$(GREEN - SWIR1) / (GREEN + SWIR1)$	Median
	NDWI _m	NDWI Modified (McFEETERS, 1996)	$(GREEN - NIR) / (GREEN + NIR)$	Median
	AWEI _{sh} *	Automated Water Extraction Index – Shadow (Feyisa <i>et al.</i> , 2014)	$BLUE + 2.5 * GREEN - 1.5 * (NIR + SWIR1) - 0.25 * SWIR2$	Median
Bare Soil indices	BSI	Bare Soil index (Rikimaru; Roy; Miyatake, 2002)	$((SWIR1 + RED) - (NIR + BLUE)) / ((SWIR1 + RED) + (NIR + BLUE))$	Median
	NBR	Normalized Burn Ratio (Key; Benson, 2006)	$(NIR - SWIR2) / (NIR + SWIR2)$	Median
	NDMI	Normalized Difference Moisture Index, also referred as MNWI or NDUI (Gao, 1996)	$(NIR - SWIR1) / (NIR + SWIR1)$	Median
Spectral Mixture Analysis (SMA) calculated from bands	GV	Green Vegetation	Endmembers [0.0119, 0.0475, 0.0169, 0.6250, 0.2399, 0.0675] respective to each band	Median
	NPV	Non-Photosynthetic Vegetation	Endmembers [0.1514, 0.1597, 0.1421, 0.3053, 0.7707, 0.1975] respective to each band	Median

Type	Name	Description	Equations (if applicable)	Statistics
['BLUE', 'GREEN', 'RED', 'NIR', 'SWIR1', 'SWIR2'] and derived indices (Souza; Roberts; Cochrane, 2005)	SOIL	Bare Soil	Endmembers [0.1799, 0.2479, 0.3158, 0.5437, 0.7707, 0.6646] respective to each band	Median
	CLOUD	Cloud	Endmembers [0.4031, 0.8714, 0.7900, 0.8989, 0.7002, 0.6607] respective to each band	Median
	GVS	Shadowed GV	$GV / (GV + NPV + SOIL)$	Median
	SHADE	Shade	$abs((GV + NPV + SOIL) - 100)$	Median
	NDFI	Normalized Difference Fraction Index (mixing components)	$(GV - (NPV + SOIL + CLOUD)) / (GV + NPV + SOIL + CLOUD)$	Median
Spectral Mixture Analysis (SMA) calculated from bands ['BLUE', 'GREEN', 'RED', 'NIR', 'SWIR1', 'SWIR2'] with Global Endmemembers Components (Small; Milesi, 2013)	SUBS	Substrate (Soil + Built-up)	Endmembers [0.178,0.337,0.458,0.559,0.683,0.645] respective to each band	Median
	VEG	Vegetation	Endmembers [0.030,0.060,0.031,0.669,0.240,0.096] respective to each band	Median
	DARK	Water + Shade	Endmembers [0.019,0.010,0.005,0.007,0.003,0.002] respective to each band	Median

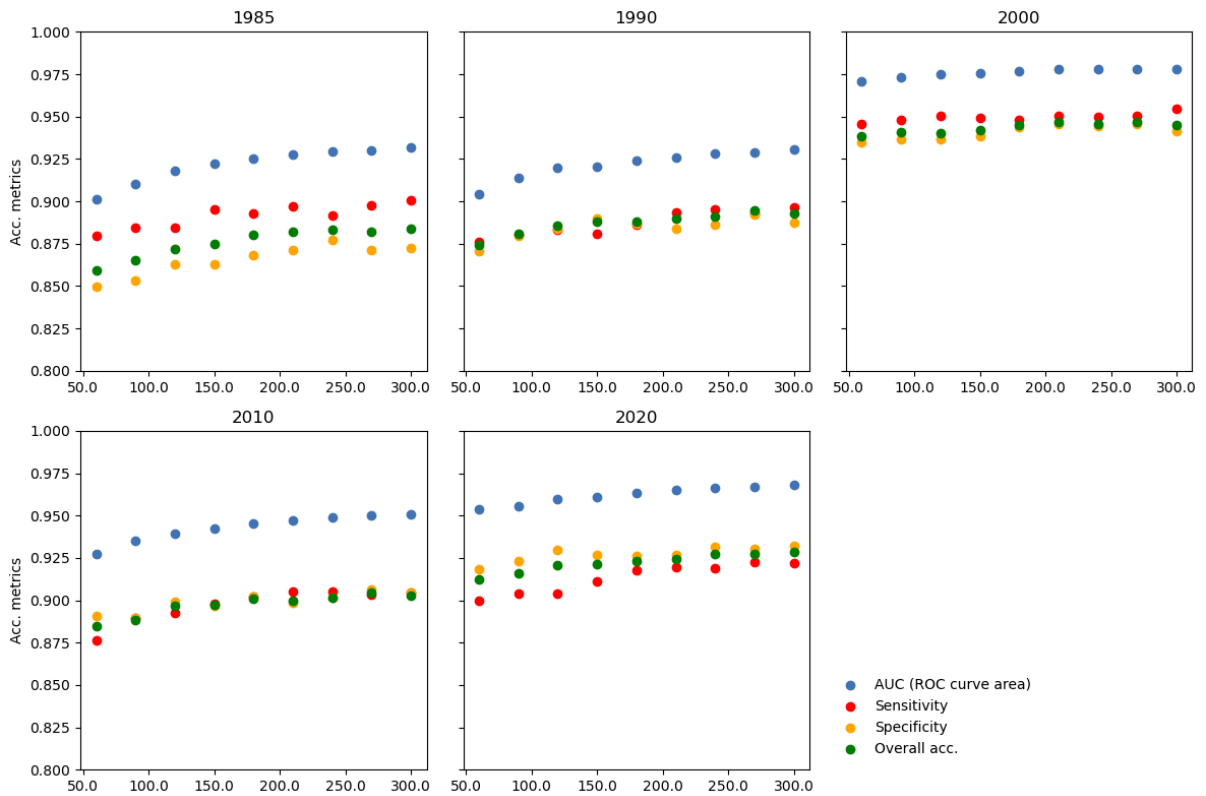
ST. 2. Bands and indices applied for urban areas classification.

* Additional indices introduced in Collection 10; all other indices and bands were previously used in Collection 9.

ST. 3. Standard mosaic used for sample's quantity analysis.

Type	Band, index name
Landsat bands	BLUE
	GREEN
	RED
	NIR
	SWIR1
	SWIR2
Vegetation indices	NDVI
	EVI
	EVI2
	SAVI
Water	MNDWI
	NDWI _m
	AWEI _{sh}
Urban areas	NDBI
	UI
	BSI
	NDRI
	BAI
	EBBI

SF. 1. Samples quantity analysis summary.

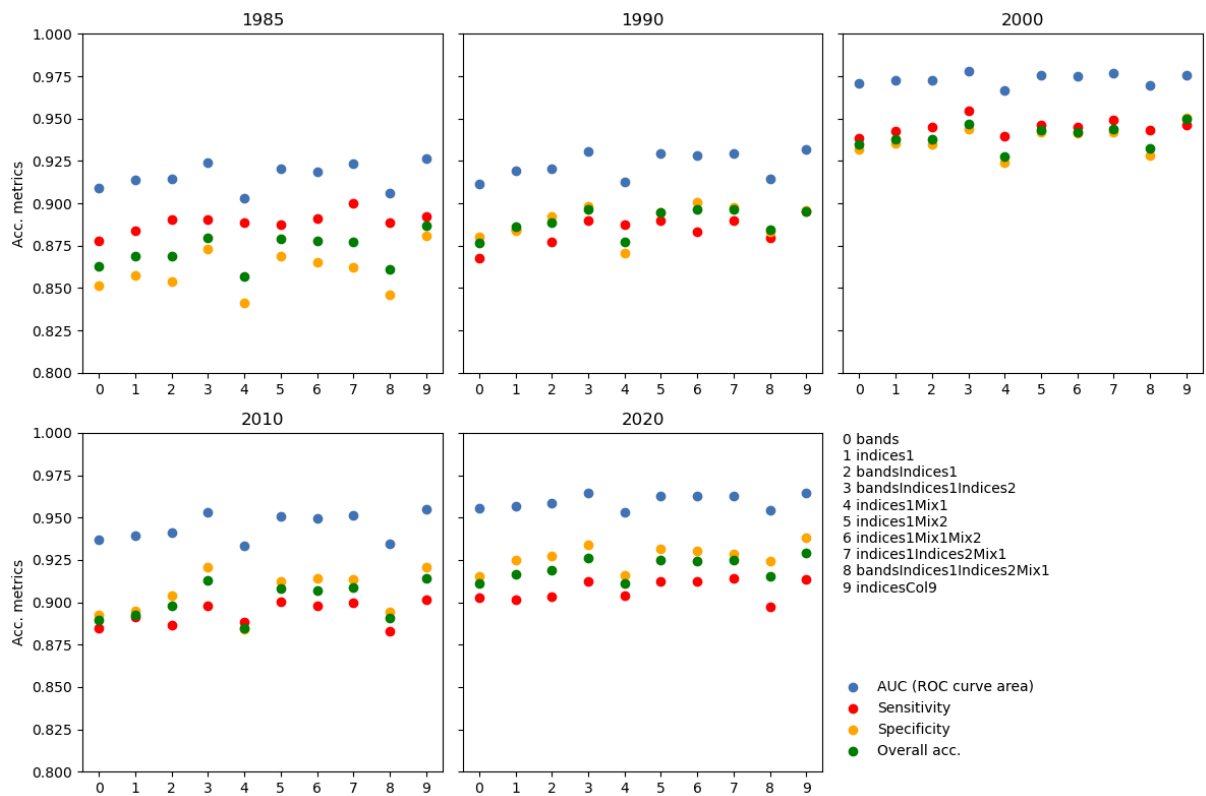


The graphs show sample quantities (x-axis) and selected metrics (y-axis) for each studied year. The results refer to the set of grids analyzed for Brazilian capitals.

Set	Type	Indices list (defined in table ST2)
Bands	Landsat bands	BLUE, GREEN, RED, NIR, SWIR1, SWIR2
Indices 1	Vegetation	NDVI, EVI, EVI2
	Water	MNDWI, NDWI _{im} , AWEI _{sh}
	Soil, urban	NDBI, UI, BSI,
Indices 2	Soil, urban	EBBI
Mix 1	Spectral mixture 1	GV, NPV, SOIL, CLOUD, GVS, SHADE
Mix 2	Spectral mixture 2	SUBS, VEG, DARK
Indices Col. 9	All indices used in MapBiomass Collection 9	All indices used in MapBiomass Collection 9 added with AWEI _{sh}

ST. 4. Mosaic compositions evaluated (mosaic refinement).

SF. 2. Mosaic evaluation.



The graphs show that different mosaics performed similarly, mainly for the cases 5, 6, 7, and 9. The mosaic 9 was selected for consistency with previous MapBiomass collections.